IDENTIFYING ENHANCED URBAN HEAT ISLAND CONVECTION AREAS FOR INDIANAPOLIS, INDIANA USING SPACE-BORNE THERMAL REMOTE SENSING METHODS

Kelly D. Boyd

Submitted to the faculty of the University Graduate School
in partial fulfillment of the requirements
for the degree
Master of Science
in the Department of Geography,
Indiana University

April 2015

Accepted by the Graduate Faculty, Indiana University, in partial fulfillment of the requirements for the degree of Master Science.

Master Thesis Committee

_____

Daniel P. Johnson Ph.D., Chair

_____

Jeffery S. Wilson Ph.D.

_____

Pamela A. Martin Ph.D.

ACKNOWLEDGEMENTS

First, I would like to thank Dr. Dan Johnson for his continued support over the past seven years as a mentor and educator from my undergraduate studies to my graduate career. Without his continued guidance, I would neither be the scientist, nor person I am today. I would also like to thank Dr. Jeff Wilson and Dr. Pamela Martin on their time and patience with this project over the last year. Several delays due to other commitments academically at other institutions for successful admission have hampered my completion of this project. Their guidance and support were helpful in my goal to eventually becoming a successful GIS analyst, remote sensor and climate expert.

Kelly D. Boyd

IDENTIFYING ENHANCED URBAN HEAT ISLAND CONVECTION AREAS FOR INDIANAPOLIS, INDIANA USING SPACE-BORNE THERMAL REMOTE SENSING METHODS

Heat is one of the most important factors in our atmosphere for precipitation (thunderstorm) formation. Thermal energy from local urban land-cover is also a common source of heat in the lower atmosphere. This phenomenon is known as the urban heat island effect (UHI) and is identified as a substantial cause to a changing climate in surface weather modification. The proceeding study investigates this connection between the UHI and surface weather using remote sensing platforms A ten-year analysis of the Indianapolis UHI and thunderstorms were studied from the summer months of May, June, July, August and September (MJJAS) from 2002 until 2011. LANDSAT space borne satellite technology and land-surface based weather radar technology was used in this analysis for thunderstorm investigation. Precipitation areas identified from land-based NEXRAD WSR-88D technology were used to identify convection from non-synoptic forcing and non-normal surface diurnal heating scenarios. Only convection appearing from the UHI were studied and analyzed. Results showed twenty-one events over eighteen days with the year 2005 and 2011 having the largest frequency of events. The month of August had the largest concentration with seven events during the late afternoon hours. UHI results showed July had the largest heat island magnitude with April and September having the lowest magnitude in UHI temperatures. Three events of the twenty-one storm paths did not had a significant mean temperature difference in the heat island below the storm reflectivity. The nineteen storm paths that were significant had a warmer area underneath storm path development by an average 6.2°C than surrounding areas. UHI initiation points showed twelve of the twenty-one events having statistically significant differences between 2 km initiation areas and the rest of the study areas.

Land-cover results showed low intensity developed areas had the most land-cover type (48%) in the 2km initiation buffer regions.

TABLE OF CONTENTS

LIST OF TABLES

LIST OF FIGURES

LIST OF FORMULAS

I. INTRODUCTION

Heat is one of the most important factors in the movement of energy on the planet. Furthermore, thermodynamically driven processes of convection in our atmosphere are one efficient method at dissipating heat in our lower climate system. Using the second law of thermodynamics, heat producing sources dissipate energy by moving higher concentrations of energy in the lower troposphere to areas of lower temperature into the upper atmosphere by air movement (Tsonis 2007). This known law, along with anthropogenic activities during the last two-hundred years, has allowed excess heat and energy to be released into the lower atmosphere via land-cover change, carbon driven-combustion and urbanization. Therefore, one can conclude that man-made processes allow for increased heat and higher energy movement through the troposphere over time. These increased activities of heat advection can affect weather and climate in human areas. Urban heat islands (UHI), are one main land-cover source of heat release into the lower atmosphere by human-kind. Additionally, if the atmosphere contains copious amounts of moisture, precipitation and thunderstorms may form as a result from surface activities. Moreover, urbanization has increased dramatically across the globe and the United States (U.S.) over the last century. According to a United Nations report, 82% of the U.S. population lives within an urban area (United Nations 2007). In this same report it was suggested the trend of urban growth is expected to grow well into the later portion of the 21st century, with predictions as much as 90% of the U.S. population living within a city by 2050. Taken together, UHIs are expected to grow spatially, increase in higher temperature magnitudes between rural areas and become more predominate in land-cover type as the climate warms across the planet.

Previous studies have linked connections between urban areas and precipitation modification (Changnon et al., Bornstein et al. 1990, 1981, Bentley et al. 2010, Ashley et al. 2012). Most of these studies have examined the urban environment at a much larger scale by examining multi-regional or multi-city approaches (Niyogi et al 2011, Scheitlin et al 2010, Shepherd et al 2002). However, research at the micro or meso-gamma scale have been neglected

in recent literature when determining whether certain UHI temperature regions within inter-urban areas are more responsible for increased precipitation within and around cities. In addition, higher spatial and temporal resolution UHI/land-cover data is needed for integration into weather and climate models for future prediction of precipitation events. The complex heterogeneity of the urban surface allows for further growth and usage in the urban climate modeling community.

In addition to future prediction, a need still exists to understand the possible causes of the dramatic increase of precipitation downwind of cities due to possible UHI affects. Precipitation produced from UHI can cause flooding in low-laying urban areas, can increase ground water pollution run-off into area water bodies and can dramatically increase moisture in agricultural fields downwind of cities. In addition to rainfall, thunderstorms in themselves produce lightning, which can produce fires, power outages and raise the potential of lightning strikes to persons located within a city. The following analysis attempts to examine precipitation in a micro-geographic sense within an urban environment using remote sensing methods first to identify increased areas of warmer land-cover and subsequently to determine the temperature magnitude of UHI in Indianapolis, Indiana for these events to take place.

II. LITERATURE REVIEW

This analysis attempts to understand the role of heat from the Indianapolis UHI on convection and thunderstorms. Over the last 40 years, several past attempts have made advancements on the subject of urban-modified thunderstorms. In addition, UHI remote sensing technology has grown tremendously and weather radar technologies have grown throughout this four decade time period. These two areas of scientific advancement have allowed geographers to understand the theoretical role of the UHI on the physical environment. This chapter highlights those advancements, past attempts and successes over UHI research and urban-modified precipitation over the past few decades.

The initial observation of the UHI effect was first mentioned by Luke Howard in London in the 1833 in his book: *The Climate of London*. Howard noticed that interior London was always warmer than the surrounding rural locations by 1.6°C (Mills 2008). Howard described how the city of London was "surrounded by an ocean of vegetation," therefore giving way to describing the city as an island of heat, the urban heat island. A myriad of studies since Howard have attempted to understand the heterogeneity, spatial layout and the intensity of urban heat islands. Most notably, Leonard Myrup's and Robert Bornstein's numerical modeling of the heat island in the 1960s and Tim Oke's research in the 1970s and 80s with surface energy fluxes and geometry of cities in relation to heat centers created the framework of discourse (Myrup 1969; Bornstein 1968; Oke 1973; Oke 1981). Satellite-based studies of UHIs did not begin until the 1970s with Rao (1972), Carlson et al. (1977) and Price (1979). These researchers were the first to utilize space-borne technologies to study urban areas. Some of these platforms included the Television Infrared Observational Satellite (TIROS), Very High Resolution Radiometer (VHRR), Heat Capacity Mapping Mission (HCMM), Landsat Thematic Mapper (LANDSAT-TM and ETM+) and Moderate Resolution Imaging Spectroradiometer (MODIS). Since the 1970-80s the use of

space-borne remote sensing technologies have risen dramatically in measuring the urban heat island of cities across the world.

Observational evidence suggests three main theories on why thunderstorms develop and are altered by the urban environment. These theories include: (1) increased anthropogenic heat release from the UHI (Shepherd 2002); (2) increased surface convergence due to urban roughness lengths (Oke 1987); and (3) higher concentrations and sizes of giant cloud condensation nuclei (GCCN) from urban combustion (Rosenfeld 2003). All three forcing's imply that the natural process of convection is amplified or produced from the urban environment. The first two theories concentrate on the role of dynamic forcing while the third hypothesis focuses on the urban microphysical process of aerosols.

Most cities are surrounded by vegetative land surfaces, which absorb incoming solar radiation (insolation). The interaction between urban and rural temperatures allows for evapotranspiration differences and yield to lower land-surface temperatures. In contrast to rural areas, urbanized areas have various land surfaces with various elevated albedo and emissivity values throughout the complex landscape. These urban reflectors, blackbodies, and grey-bodies either reflect (e.g. glass, concrete) or absorb (e.g. asphalt, shingles) incoming solar radiation throughout the environment. The urban surface allows for higher land-surface temperatures to exist given a large spatial area of solar absorbing surfaces and blackbodies (Oke 1987). Eventually, the high solar absorbing urban surface will release heat back into the environment. This simultaneous process releases heat through conduction into the atmosphere where heat is then eventually moved via convective processes throughout the lower atmosphere. Ultimately, the lower warming of air in the urban boundary layer allows local instability to occur above and around a city. In some cases, if the urban environment absorbs enough solar radiation, a strong temperature and pressure gradient between the urban core and rural areas can create a convergence zone (Figure 2.1). A circular flow is then established permitting cool air from rural areas to be moved toward the warmer urban core, thereby pushing unstable air aloft.

After natural daytime heating of the lower atmosphere and warming of the UHI surface, air parcels begin to rise and cool to the saturation point allowing clouds to form. If excess moisture is present in these "urban air parcels", precipitation and thunderstorms can be produced over large urban areas. Therefore, precipitation tends to form more predominately over urban areas. Many other theories suggest factors such as heat and moisture emissions by industrial plants, automobiles and building air conditioning units can also contribute sensible and latent heat to the environment aiding in additional parcel lift (Cotton and Pielke 2007).

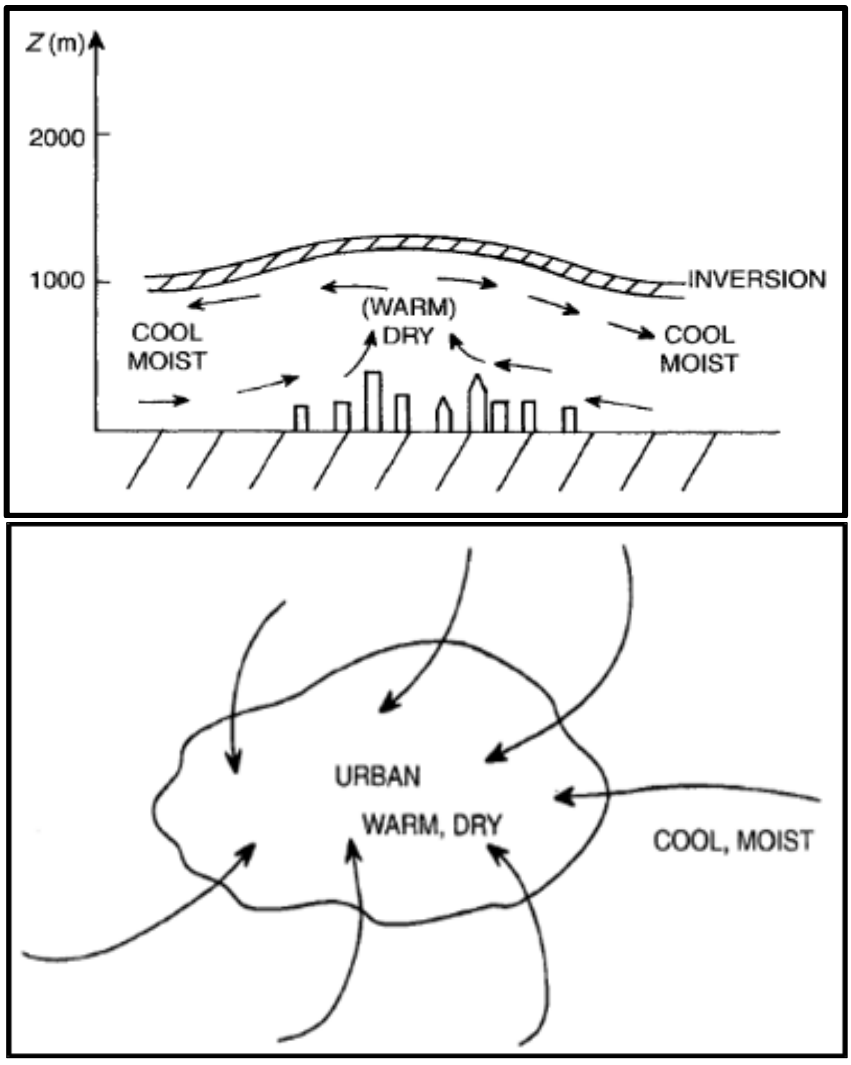

Figure 2.1 (Top): Horizontal visual representation of an urban area convergence area. (Bottom) Vertical representation of an urban convergence zone (Cotton and Pielke 2007)

Since diurnal heating of the surface tends to take place in regions of large air subsidence, air-mass thunderstorms (ordinary/single-cell) tend to be the predominate phenomenon studied when examining precipitation and urban land-cover. According to one recent study, air-mass thunderstorms tend to be initiated to a higher degree by convergence forcing mechanisms than by any other possible forcing mechanism during the summer months of June to August due to strong solar radiation (Bentley et al. 2010). The recent theory suggests that by studying thunderstorms in a low mechanical forcing environment during strong solar heating, researchers can determine what effect, if any, urban areas or the UHI have on precipitation and thunderstorms. Thus, if observational findings and measurements can be made between urban-atmosphere interactions, the scientific community can better understand the role of these processes and apply similar theories on much larger scales.

Additional research has suggested that if wind velocities are slightly elevated aloft, the resulting convergence zones and areas of convection may be advected downwind or along the edges of cities (Stallins and Bentley 2006; Bornstein and Lin 2000). Due to this advection, precipitation tends to be heavier downwind of urban areas and not directly over the cities. Other studies have shown thunderstorms bifurcate or split around urban centers and reform stronger downwind of cities (Niyogi et al. 2006). Figure 2.2 shows a case study in which a thunderstorm split around the city of Indianapolis on June 13, 2005 (Niyogi et al. 2011).

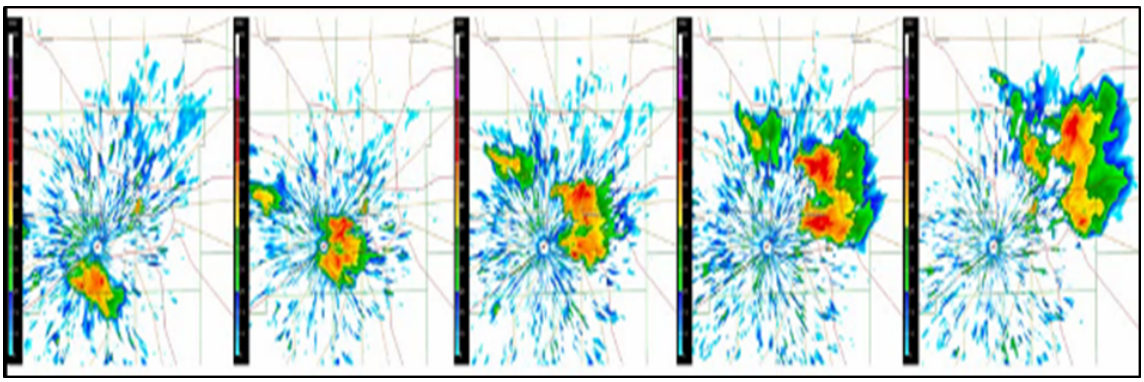

Figure 2.2: An example of a thunderstorm splitting over the metropolitan area of Indianapolis, IN (Niyogi et al. 2011)

Niyogi et al. (2011) completed additional research on thunderstorms and the greater Indianapolis area from May 2000 until August 2009 and found that 60% of the 91 thunderstorms studied changed composition and structure after moving over the city center. Additionally, Niyogi et al. found 71% of day-time thunderstorms were impacted compared to only 25% of nocturnal thunderstorms. The study concluded that Indianapolis impacts thunderstorms as diurnal convection moves over the metropolitan area.

Two recent observational studies on the UHI/thunderstorm linkage, which were directly related to the preview of this study by Shepherd (2002) and Dixon and Mote (2003). Shepherd (2002) found precipitation higher downwind of five U.S. cities (Atlanta, Montgomery, Dallas, Waco and San Antonio) over a two-year period using remote sensing technologies. The Shepherd study was one of the first studies to use satellite technology [the Tropical Rainfall Measuring Mission (TRMM) satellite] to observe the direct connection between remotely-sensed UHIs and precipitation. The increased rainfall amounts downwind of UHI locations were found to be up to 28% higher than upwind areas of the cities. Thermal imagery from LANDSAT confirmed the UHI through surface temperature imagery and subsequently follows the connection of rainfall accumulation downwind of the urban locations. Shepherd also found a 5.8% increase of rainfall accumulation extending orthogonal and to the right of the main prevailing flow within 50 km of the UHI.

Dixon and Mote (2003) examined the spatiotemporal patterns of thunderstorms as well as the overall synoptic-air mass environments needed for UHI induced thunderstorm events for Atlanta. The hypothesis of the study was to test if thunderstorm events were connected to the intensity of the UHI. The Dixon study was one of the first to use urban land-cover to determine if there were patterns of thunderstorm initiation. The study found a majority (56%) of thunderstorms formed within 5 km of transportation networks, especially areas with new development. Dixon and Mote (2003) concluded from 20 days that 37 urban initiation locations occurred over a five-year period and that low-level moisture was more important factor in

thunderstorm formation than the heat intensity given off by the UHI. The study found July had the highest average thunderstorm initiation periods with twelve events followed by August and then May. Most UHI-based thunderstorm events were found to take place just after midnight local time when moist tropical air masses [moist tropical (MT) or moist moderate (MM) SCC types] were in place, with the majority of thunderstorms (56%) developing within a 5 km buffer around local interstate highways. Additionally, a majority of these thunderstorms developed close to the urban center of Atlanta (Cobb County).

Another theory why thunderstorms are associated with cities centers on variations in roughness lengths. Roughness length is a parameter to measure the complexity of a surface by averaging land-surface feature heights compared to the square area of land-surface features (Oke 1987). Higher land-surface values indicate a rougher surface, meaning higher turbulence and slower wind speeds. A roughness length value closer to zero indicates a flat, more homogenous surface allowing for elevated wind speeds both at the surface and aloft. Urban environments have a complex surface allowing for slower wind speeds due to higher roughness lengths (Figure 2.3). As wind flow slows, the wind is either directed around or over a land-surface feature. As a result, the perturbation displaces air above and on the leeward side of an urban object. In some cases, the entire urban area (Figure 2.4) may impact airflow around a city. The “urban” perturbation in air displacement is similar to the process of leeward cyclogenesis at the synoptic scale with natural terrain but in these instances at a meso or local scale with anthropogenic surfaces. The spin or eddies induced by the wake of the man-made urban topography can cause air to converge and rise thereby allowing convection to take place downwind of urban objects such as large-tall buildings.

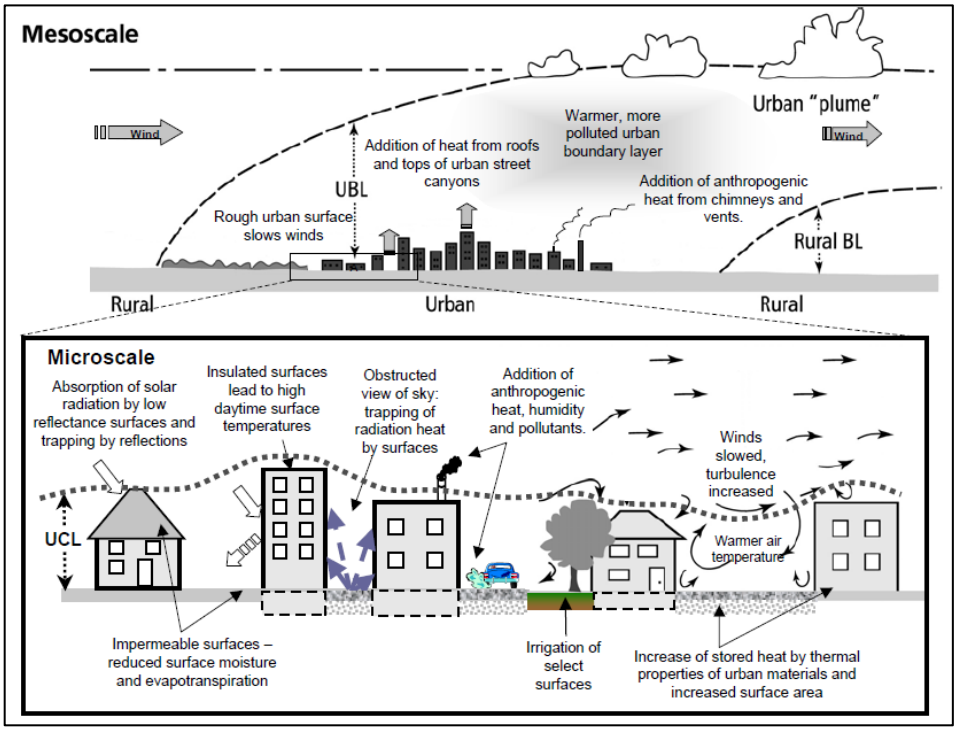

Figure 2.3: A vertical diagram illustrating at various scales the effect of topography on wind and chaotic flow within an urban boundary layer (UBL) and urban canopy layer (UCL). Increased turbulence can induce convective eddies within a urban location (Oke 1997)

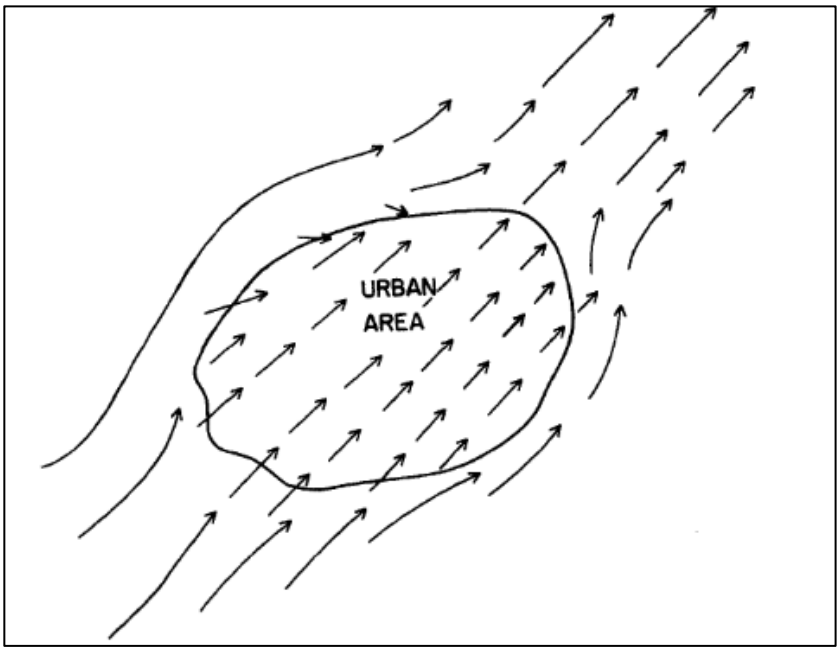

Figure 2.4: A diagram displaying downwind convergence from an urban area. Notice the size of wind flow vector arrows over the city compared to wind vectors upwind, around and downwind of cities. The downwind areas are conducive to convection and thunderstorms (Cotton and Pielke 2007).

Many studies have confirmed the theory of urban convergence through observational field campaigns throughout the United States. The urban convergence theory was first proposed and studied in the 1970s through the observational METROMEX investigation of St. Louis (Changnon 1981). Heavier precipitation was found downwind of the commercial business district and northeastern portions of St. Louis. Changnon also discovered the urban boundary layer was 100 to 400 meters higher than the surrounding rural areas. Changnon et al. also found air mass or ordinary thunderstorms were found to occur 116% more frequently downwind of St. Louis than in other rural areas around St. Louis. In another study for New York City (NYC), Loose and Bornstein (1977) found cold fronts and mesoscale boundaries tended to slow down upwind of the city and speed up downwind of the city. Higher roughness lengths and surface drag can explain the phenomenon of air boundary advection modification from urban-building topography.

Thunderstorms have been found to split due to wind flow through the city. Bornstein and LeRoy (1990) first found that NYC split thunderstorms moving over the city and that thunderstorms initiated over cities during calm synoptic flow days. Bornstein and LeRoy also found radar reflectivity returns were higher along the edges and downwind of the city with lower precipitation reflectivity returns over the city indicating a possible split and lapse in precipitation over NYC. In Atlanta, Bornstein (2000) confirmed thunderstorms tend to split, initiate or develop downwind of the urban center. Studying wind and precipitation across the Atlanta metro area from July 26-August 3, 1996, Bornstein et al. found thunderstorms formed primarily over convergence zones for three events over the eight day period at around 6:30 am EDT, 8:45 a.m. EDT and 2:45 p.m. EDT. Convection was found to occur along strong UHI boundaries with rural regions surrounding Atlanta during calm synoptic flow periods with surface winds below 4 m s-1. Weak synoptic flow indicates a mixed role of both forcing mechanisms (the UHI and UBL winds) play a vital role in thunderstorm formation around cities.

Numerical models have confirmed theories of airflow impacting convection downwind of urban areas (Thielen et. al. 2000; Rozoff et al. 2003; Adegoke and Gallow 2004). Early urban numerical models used mesoscale models and incorporated urban land cover data to test current roughness length variations. Thielen et al. (2000) was one of the earliest contemporary researchers to model the urban boundary layer in two-dimensions. Thielen examined two events over Paris, France during June 1999 to determine the maximum spatial extent in which to encompass heat fluxes and roughness lengths efficiently for a city initiating precipitation. The study determined two important factors for future numerical modeling: the largest scale possible scale should be in the meso-gamma scale (largest spatial extent should be less than 20km) and urban precipitation events should be studied within a 4 hour period or less when studying events. Thielen also determined that when the UHI is weak, surface sensible heat fluxes, convergence, and buoyancy variations were more important downwind from a city. The Thielen study concluded precipitation downwind or on the lateral edges of cities were a more important factor to examine than thunderstorms forming directly over the urban heat core.

Rozoff et al. (2003) also tested the theory of urban surface convergence due to increased roughness through numerical modeling by simulating a 1999 St. Louis storm event. The study found that convergence on the leeward side of the city exhibited an important role in initiating thunderstorms. Rozoff et al. concluded that increased momentum drag over the city induces convergence on the windward side of the city, but it does not necessarily always cause thunderstorm formation. Momentum drag is caused by wind shear and pressure differences around an object (Oke 1987). The study concluded that urban heat fluxes, wind flow, frictional drag and vertical velocities are important factors when examining convection and thunderstorms around cities. Currently, researchers are concentrating on developing specific micro-scale urban models to test site-specific roughness length variations impacts on convection at a higher resolutions (Miao et al. 2009; Salamanca et al. 2011; Niyogi et al. 2011). A great need exists in

identifying events in which thunderstorms are impacted by cities for simulation in numerical modeling to determine the connection between thunderstorms and urban areas.

A third theory has suggested that large distributions of giant cloud condensation nuclei (GCCN) in urban plumes help the collision and coalescence process consequently allowing for precipitation and thunderstorms to form. Updrafts from the urban environment are thought to cause GCCN to reach higher levels of the atmosphere thereby allowing clouds to become glaciated (Figure 2.4). The "urban clouds" identified by Rosenfeld, frequently live longer, grow higher and last longer than typical "non-urban clouds" or clouds encompassing much smaller CCN (Cotton and Pielke 2007). Other studies have found GCCN aerosols from urban environments can suppress rainfall from GCCN (e.g., Rosenfeld 2000; Ramanathan et al. 2001).

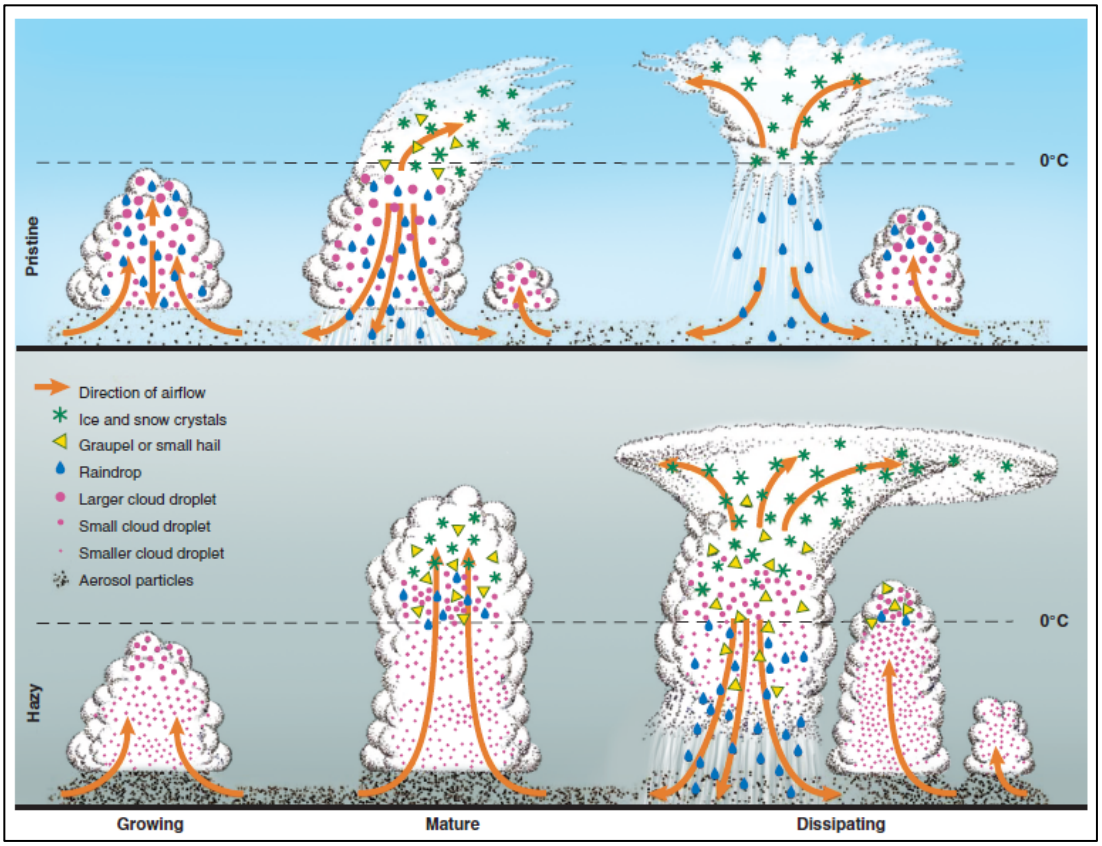

Figure 2.5: Above/top image displays a convective scenario with small and low concentrations of CCN. Below/bottom diagram shows a convective scenario with high concentrations of GCCN allowing for taller, glaciated, longer-lasting clouds (Rosenfeld 2007).

Ramanathan et al. (2001) has suggested that aerosols suppress precipitation since a significant portion of aerosols decrease the amount of solar radiation reaching the surface, which in turn evades warming thus reducing surface heating and evaporation needed for cloud formation. The study continues by stating aerosols retain heat from solar energy and consequently warming the air aloft. Warming air aloft stabilizes the surrounding air by suppressing parcel lift and prohibiting convection through inversions. Other suppressing theories suggest certain sizes and concentrations of CCN from aerosols prohibit the conversion of cloud droplets into rain droplets, which are slower to coalesce into hydrometeors (Gunn and Phillips 1957). In more recent studies using satellites, researchers have observed urban and industrial air pollution may completely suppress precipitation with carbon-based smoke from forest fires (Rosenfeld 2000; Rosenfeld et al. 1999).

Additional theories show carbon-based aerosols can aid in convection. Combustion within urban environments follows similar convection processes seen in warmer environments (e.g. burning smoke in the Amazon Forest). The burning of carbon-based material can actually invigorate convective processes by adding excess aerosols into the atmosphere (Andrea et al. 2004). Figure 2.4 shows the high concentrations of aerosols in urban environments can lack efficient cloud droplets coalescence on carbon based GCCN. Therefore, GCCN allow more water vapor to collect through longer condensation processes within the cloud within urban environments. Thus, the process of longer cloud nucleation may be applicable to warm urban environments with large aerosol concentrations (Shepherd 2005). Aerosols can initially suppress the onset of precipitation in warm convective clouds that develop in moist tropical environment; as a result, downdrafts are delayed allowing for stronger downdrafts later in the convective life-cycle of thunderstorms, which can then induce other stronger convection through outflow boundaries. Suppressed downdrafts of thunderstorms allow clouds to uptake more water vapor and allow a more efficient rimming process (Rosenfeld 2008). Increased rimming of

hydrometeors allows for greater cloud electrification and potentially more lightning strikes around cities as noted in some studies (e.g. Rose et al. 2008).

One observational study to help determine the relationship between precipitation, CCN, and urbanization was conducted in Phoenix, Arizona. Diem et al. (2003) studied precipitation data from 1890 until 2000 for the Phoenix Metro Valley to determine if precipitation was higher downwind of the city than other basins around the city. The study concluded through statistical means that precipitation was higher during 1950 to 2000 during the rapid urbanization of Phoenix, and it was due mostly to increased water vapor and aerosols from irrigation as well as increased pollution-generating activities.

In a more recent study using modeled simulations, van den Heever et al. (2006) found a more plausible link between cities and thunderstorms. The study for St. Louis used a June 1999 event initially used by Rozoff (2003) to test if aerosols played a role in thunderstorm events rather than dynamic forcing from urban land-cover. It was found that the convergence effect of the UHI has more to do with thunderstorms developing rather than aerosols in controlled simulations. The study however noted GCCN and excess aerosol concentrations from the St. Louis metro area did enhance cloud water and rain formed more rapidly than in the control simulation in which only natural aerosols were present, but the excess GCCN observation was observed after thunderstorms were initiated by the urban environments. Van den Heever and her team also noted stronger updrafts which was a result of a longer autoconversion rate. The study also noticed higher electrification of clouds with excess lightning strikes than scenarios without excess concentrations of aerosols. The research paper did note the excess electrification case was conducted on only one location with certain atmospheric parameters so further modeling and more events at other locations are needed to model.

In one of the first observational studies and non-numerical simulation of aerosols and precipitation, Lacke et al. (2009) discovered when aerosol concentrations were higher for the city of Atlanta that the precipitation was heavier downwind of the city. The study used two years of

EPA air monitoring data studying how precipitation varied with aerosol concentrations by certain days of the week. The team found high aerosol days had higher convective available potential energy (CAPE) values, lower convective inhibition (CIN), and a slightly shallow mixing layers compared to low aerosol days. Lacke et al. found Thursday had the highest concentration of particulate matter (PM 2.5μm) with Monday and Thursday having the largest area of significantly different precipitation than any other day of the week.

In the proceeding analysis, ordinary thunderstorms was studied in and around Indianapolis area from May 2002 until September 2011 for a ten year period given the large amount of studies who studied the same period (Dixon and Mote 2003; Shepherd 2005). A longer study period was selected to capture events during the transitional periods (spring and fall seasons) and to gather a longer time series than in previous studies. Several deficiencies exist with past studies outlined in the preceding chapter. Hence further research is needed in the following areas. First, a majority of earlier studies only examine a short interval of time. Most, if not all recent studies, analyze the relationships of precipitation and cities in less than a five-year time period or only one to two selected events. A longer time period and sample size is needed to determine patterns on thunderstorm formation due to the UHI. A second major deficiency involves geography; most prior theories were concluded on only one or a few common cities (e.g. Atlanta, New York City and St. Louis). Other locations throughout North America are needed to gather observational data to determine if varying geographies of the UHI and spatial layouts of cities have different impacts on convection. Finally, most studies have researched the regional or multi-city approach throughout literature. No in depth study of a city's UHI temperature intensity over time and space using space-borne remote sensing platforms have been completed with weather radar data. This study attempts to examine the heterogeneity of temperature intensities across the Indianapolis metro area in relation to observed convection above and around Indianapolis.

III. DATA & METHODOLOGY

Ten years (2002-2011) of LANDSAT-5 thermal imagery were used and compared to convective days within close passage of the LANDSAT-5 satellite over the Indianapolis. Only convective events meeting the "air-mass" criteria with weak synoptic flow were chosen for this analysis. Thunderstorms initiated by fronts, pressure systems, troughs and outflow boundaries were eliminated from the study since forcing other than surface features initiate convection. Additionally, widespread convection days in which a majority of the study area experiences rainfall due to day-time heating will be removed from this study. The Indianapolis Metropolitan Area was selected given its location around farmland (vegetation) and the relatively low relief surrounding the area. Indianapolis is also in the mid-latitudes at approximately 40.0°N which allows sufficient insolation (incoming solar radiation) and precipitation throughout the study period months between May and September.

The UHI study area for this analysis encompasses an area within a 35 km radius buffer around the city center (Monument Circle) in downtown Indianapolis. The 35 km buffer was selected to encompass the entire Indianapolis urban footprint and to eliminate peripheral cloud cover in the 170 km by 183 km LANDSAT-5 imagery provided by the United States Geological Survey (USGS). Another major reason for selecting a 35 km study region entails the sampling of the atmosphere above the Indianapolis Metro Area. Typically NEXRAD radar samples the atmosphere in a cone-shape region originating from the NEXRAD radar site close to the Indianapolis Airport. The best radar sampling range is below 1219 m (4,000 ft.) below a radius 85 km of the radar site KIND (Figure 3.1). Therefore, to fall within the viable study range of studying precipitation below 1219 meters a study area, avoiding cloud-cover and encompassing the Indianapolis UHI, the 35 km study region is suitable for this analysis.

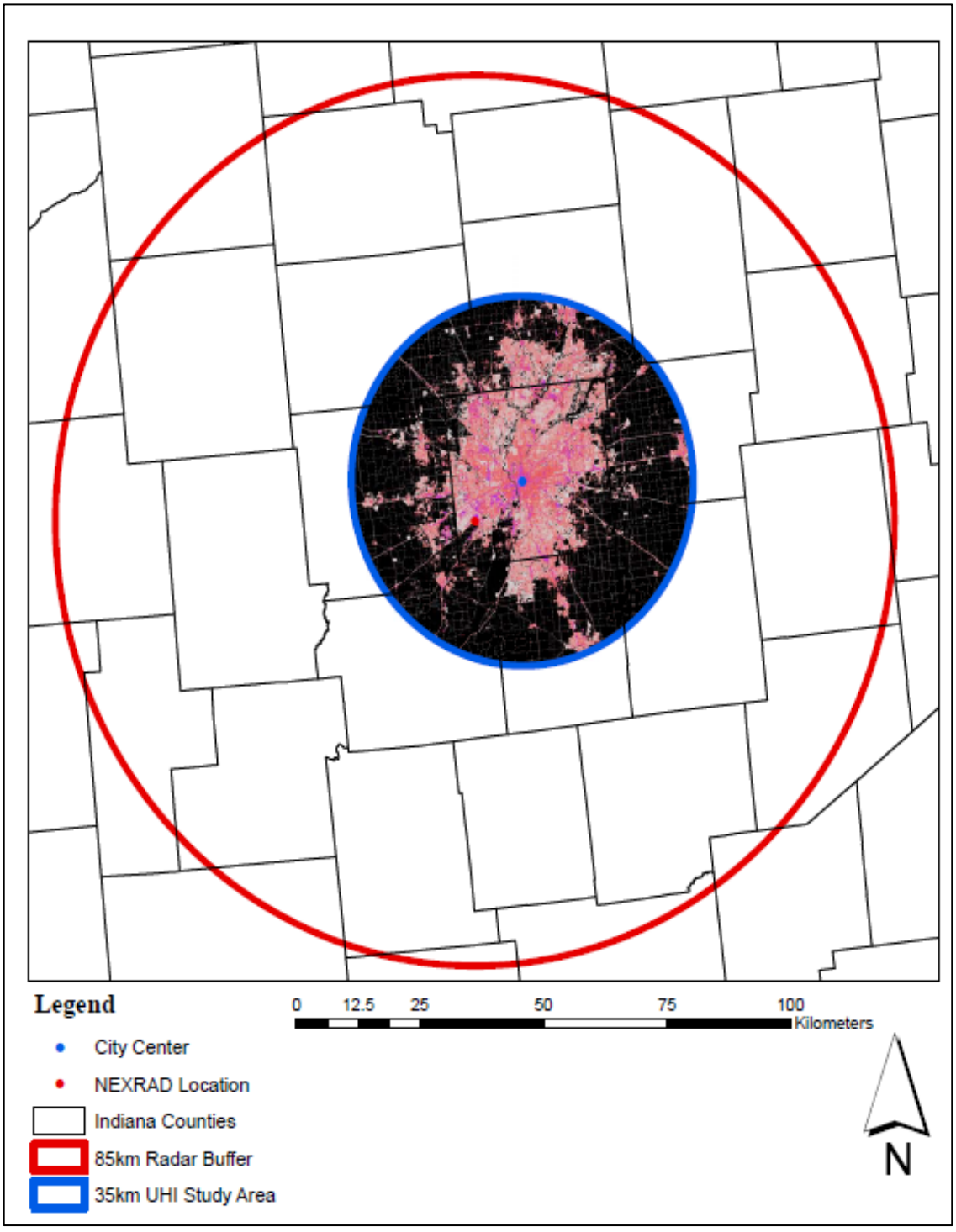

Figure 3.1: The study areas in relation to the UHI study area (blue circle) and the NEXRAD radar study area (red circle). The pink/red areas show the Indianapolis impervious surfaces (UHI) in relation to the rural/vegetative area (in black) from the National Land-Cover Dataset (MRLC 2014)

The first step of this analysis was to establish study days for possible UHI initiation events for Indianapolis. Days were selected by examining the University Corporation of Atmospheric Research (UCAR) Meteorological case study database located at http://locust.mmm.ucar.edu/ from May 1st 2002 until September 30th 2011. Archived surface and 500 hPa synoptic charts were first used to determine if synoptic forcing was present around and aloft over Indianapolis. Figure 3.2 depicts the weak-synoptic flow area needed to exist within the buffer around Indianapolis.

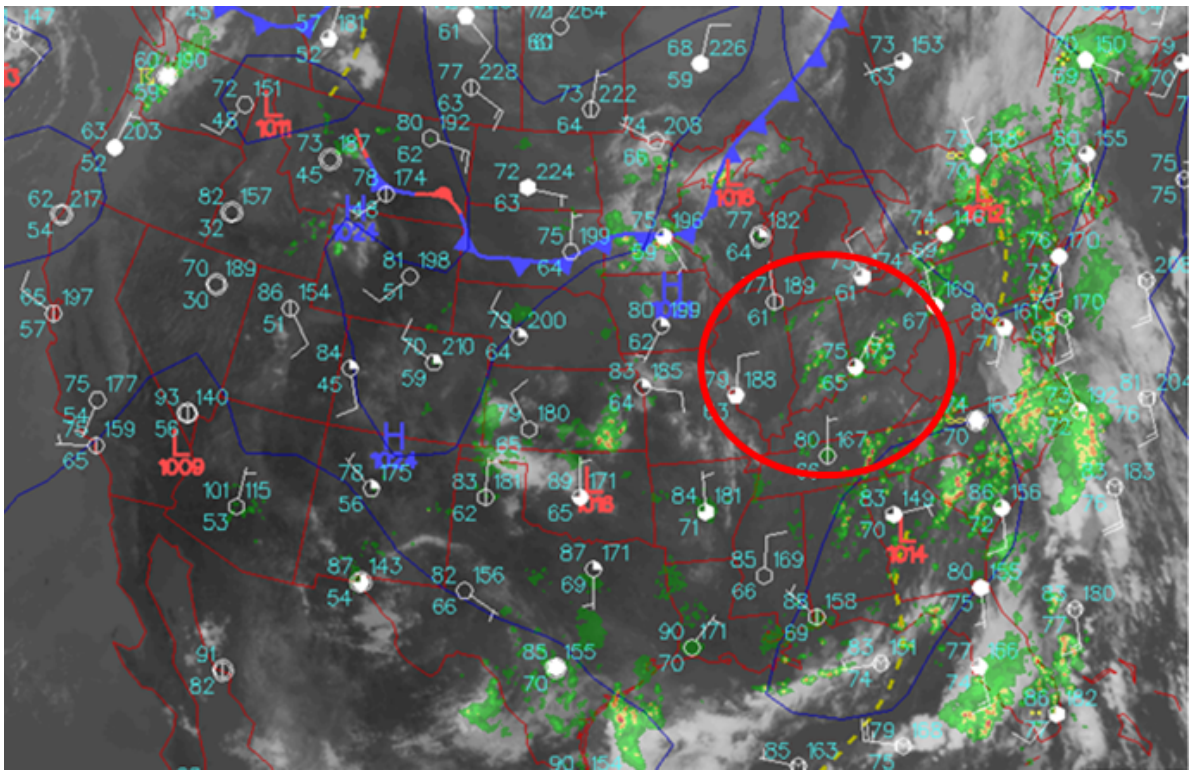

Figure 3.2: A 500km buffer around the Indianapolis Metro Area. No upper air or surface features can be located within this buffer in order to be considered viable in this analysis. The map is a synoptic weather map on September 20th 2008 (UNYSIS 2013).

The Brown and Arnold (1998) weak synoptic environment methodology uses three criteria: 1.) no synoptic surface forcing within 500 km (fronts, pressure systems, outflow boundaries, etc.); 2.) 500-hPa wind speeds with the region of less than 15 knots; and 3.) surface wind speeds of less than 10 knots. Days exhibiting these characteristics were selected for further

analysis. Next, regional radar activity from the UCAR website was studied around Indianapolis from this subset of days to determine possible precipitation from the UHI (Figure 3.3).

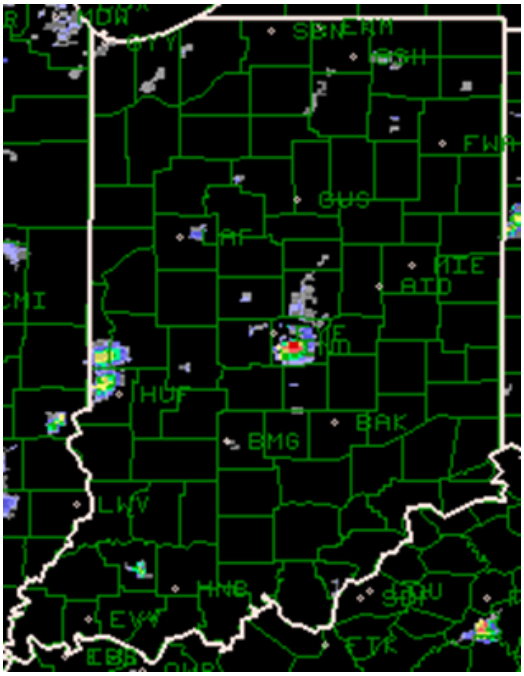

Figure 3.3: Regional NEXRAD radar depicting possible thunderstorm initiation by the Indianapolis UHI on September 2nd 2008 (radar image via UCAR 2013).

Once weak-synoptic flow/precipitation days were found from the UCAR dataset, local KIND NEXRAD radar was obtained from the National Climatic Data Center (NCDC) archived radar site located at http://www.ncdc.noaa.gov/nexradinv/chooseday.jsp?id=kind. Level II base data was downloaded and 0.5° base reflectivity was used for thunderstorm selection. Level II data has higher spatial resolution at 250 m x 250 m and at a faster temporal resolution of six minutes per scan. Level III data takes longer and has a lower spatial resolution (NCDC 2013). Raw radar data was processed in the NOAA Weather and Climate Toolkit Version 3.7.3 (WCT) and can be downloaded for free from http://www.ncdc.noaa.gov/wct/. A thunderstorm on radar by definition is NEXRAD radar reflectivity values greater than 40 decibels (dBZ) or 11.5 mm hr-1 (Bentley et al. 2012). Further, a thunderstorm for this analysis is defined as a convective area (4 to 400 sq km) in size of 40 dBZ or greater and lasting for a temporal period of at least two hours (120 minutes). The meso-gamma scale is the smallest spatial definition of a thunderstorm and therefore

will be utilized at sampling surface area below initial radar returns (Orklanski 1975). The WCT was used to process raw radar data into shapefiles that were used within a GIS program. Each six minute scan coverts all 1 km reflectivity data into a shapefile format and were filtered to only process 40 dBZ data. All scans over the lifetime of the thunderstorm over 40 dBZ were gathered and merged into one shapefile for use with LANDSAT raster data. Figure 3.4 shows the WCT processing raw radar reflectivity into shapefiles.

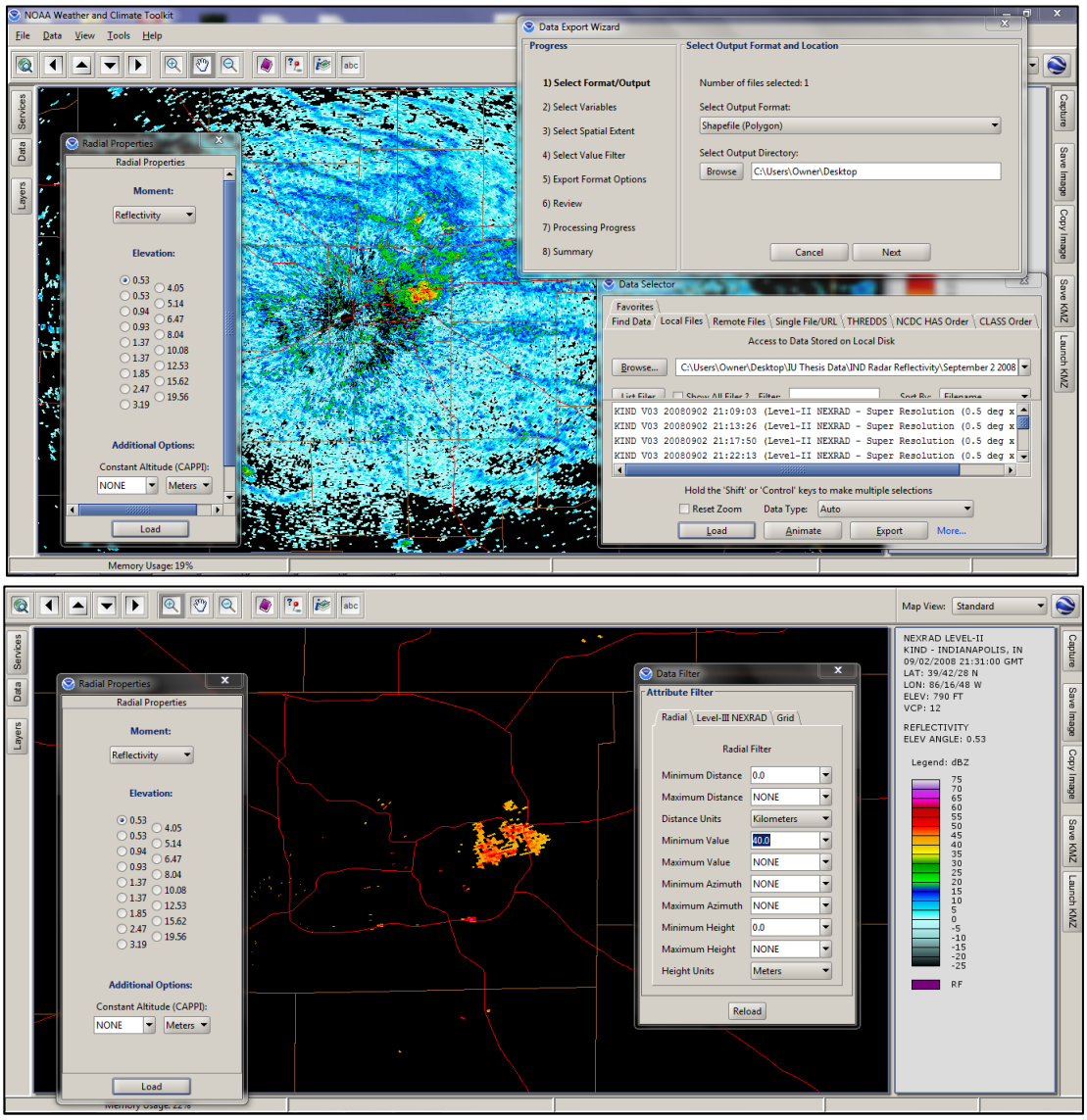

Figure 3.4: The top image depicting the NOAA WCT processing raw radar data into shapefile polygons to be used within a GIS program. The bottom image shows the resulting shapefile output of reflectivity of 40 dBZ or higher.

Thunderstorm path reflectivity and initial convective regions were identified by this radar data and both were used in the statistical analysis. Only thunderstorms (reflectivity) appearing and forming over and near the Indianapolis urban land-cover was investigated and used for thermal examination. Mean centers were calculated on initial radar reflectivity data within ArcGIS 10, and 2km buffers were formed around the initial reflectivity area. The logic behind this decision rests on the smallest scale at which a thunderstorm can exist, the meso-gamma scale (2 km x 2 km areas).

LANDSAT data was gathered and processed from http://glovis.usgs.gov/. The LANDSAT-5 platform is a passive remote sensor measuring radiation on the surface of earth in seven band channels at 30m x 30m spatial resolutions (NASA 2009). LANDSAT-5 also has a thermal band collecting data at 120 m spatial resolution. Two LANSDAT satellite images were merged in order to obtain the entire UHI of Indianapolis (Path 21 and Row 33). Both images were geo-rectified within ERDAS Earth Imagine using the Mosaic function. Days showing little to no cloud-cover in the images were used for this study. Scenes with cloud cover can bias surface temperature and skew the results of the statistical analysis. Given that the goal of the research is to measure the UHI changes over time in relation to thunderstorm activity, it is impossible to measure the heat island remotely while cloud cover from thunderstorms of interest are present over Indianapolis; therefore, LANDSAT-5 satellite imagery in close temporal proximity were used in this research. Another reason for selecting several LANDSAT-5 images was to measure the changes in the UHI over the time of the year from May to September and to track the growth of the UHI over the ten-year study period. In addition, LANDSAT-5 imagery is free to the public and has an excellent temporal record over the ten-year period.

After dates of imagery were selected, processing of the imagery began. First, the Normalized Difference Vegetation Index (NDVI) was calculated in order to determine the percent of vegetation in the two combined images. NDVI is a proportion of vegetation in an image using visible red light and near infrared. More specifically, NDVI is calculated by taking the pixel value

of near-infrared light (band 5) and subtracting the red light (band 4) pixel value and then divided by the sum of both pixel values. Each 30-meter pixel within the images must have the NDVI calculated in order to measure surface temperature. Formula 3.1 defined by Sobrino et al. (2004) was used in processing the percent of vegetation around Indianapolis using LANDSAT-5 imagery.

$$\mathrm{NDVI} = \frac{(\mathrm{NIR} - \mathrm{VIS})}{(\mathrm{NIR} + \mathrm{VIS})}$$

Formula 3.1: NDVI calculation for LANDSAT imagery

The second step of processing LANDSAT-5 data includes calculating the percent of vegetation in each of the 30 m by 30 m pixel. Vegetation can heavily impact the surface temperature as plants for photosynthesis purposes absorb most solar energy. Percent of vegetation is difference between the NDVI pixel value calculated in the previous formula and subtracted from the minimum NDVI value $NDVI_{min}$ of 0.2 and the maximum NDVI value $NDVI_{max}$ of 0.5. The formula from Sobrino et al. (2004) for calculating the percent of vegetation is below:

$$P_v = \left[\frac{\mathrm{NDVI} - \mathrm{NDVI}_{\min}}{\mathrm{NDVI}_{\max} - \mathrm{NDVI}_{\min}}\right]^2$$

Formula 3.2: Percent of vegetation (P_v)

Next, the emissivity for the LANDSAT thermal band was calculated by using the percent of vegetation calculated in the previous formula. The emissivity or the amount of solar radiation absorbed by the surface is directly linked to the temperature of that surface using the Stefan-Boltzmann Law. Again the emissivity formula by Sobrino et al. (2004) was used in this calculation. The formula takes into account pixels that have bare soil, vegetation and a mixture of both bare soil and vegetation within the pixels.

$$\varepsilon_{TM6} = 0.004\ P_v + 0.986$$

Formula 3.3: Calculation of emissivity of thermal band 6 (ε_{TM6})

The fourth step involves the calculation of the at-sensor radiance-using band six. Spectral radiance is the amount of energy or radiation reaching the LANDSAT-5 sensor in space-based sensor. The formula for calculating spectral radiance (W sr^{-1} m^{-2}) is from Weng et al. (2004).

$$L_\lambda = \left(\frac{LMAX - LMIN}{QCALMAX - QCALMIN} \right) * (DN - QCALMIN) + LMIN$$

Formula 3.4: Spectral radiance of a satellite sensor (L_λ)

Several variables are constants in the previous formula and mainly based from the engineering of the satellite when it was built. Using the thermal band pixel values (DN), the quantized calibrated pixel values at the maximum-255 (QCALMAX), the minimum-1 (QCALMIN), the specific sensor spectral radiance at minimum-1.2378 (LMIN), the maximum-15.303 (LMAX) for the LANDSAT-5 platform, and then programming the variables in the formula allows for spectral radiance for the entire study area (NASA 2009). The radiance calculated in the previous formula assumes one emissivity value, thus another calculation is needed for converting radiance into blackbody temperatures and then eventually taking into account emissivity calculated in Formula 3.3 in yet another final formula for the actual surface temperature. First, using the blackbody temperature formula again from Weng et al. (2004):

$$T = \frac{K2}{ln\left(\frac{K1}{L_\lambda} + 1\right)}$$

Formula 3.5: Blackbody temperature (T) in Kelvin

Where K1 is a calibration constant for the LANDSAT-5 platform (607.76 watt/m^2 *ster*μm), K2 is the calibration constant of 1260.56 K, and L_λ is spectral radiance calculated in the previous formula. With all background variables, emissivity and blackbody temperatures

calculated, the surface temperature formula utilized by Weng et al (2004) was used to get the actual surface temperature in Kelvin.

$$S_t = \frac{T_B}{1 + (\lambda \times T_B / \rho)\ln\varepsilon}$$

Formula 3.6: Surface temperature (St) in Kelvin

Where the blackbody temperature (TB) is from formula 3.5, emitted radiance (λ) is a constant at 11.5μm, rho (ρ) is a proportional constant of Planck's constant, the velocity of light and the Stefan-Boltzmann constant ($\rho = 1.438 \times 10^{-2}$ mK). The resulting calculated pixel values are temperatures in Kelvin and were easily converted into degrees Celsius. The final output from this formula were temperature maps of the Indianapolis study area and in which were compared to NEXRAD radar reflectivity. LANDSAT raster pixel data of study areas were then converted into numerical data to be used within a statistical software program for statistical testing.

The researcher of this study predicts thunderstorm activity exhibited a pattern of forming over warmer areas of the UHI of Indianapolis. Statically significant results at a 95% confidence level were used to test this hypothesis by conducting several two-sample t-testing of surface temperature data. Spatial sampling of thunderstorm data were conducted under two methods. The first sample used thermal pixels directly below the convective area (or the entire storm path) from initiation to dissipation of the thunderstorm. Again, the research assumes weak synoptic flow aloft and at the surface, thus temperatures at the surface under the initial radar reflectivity are the main contributor to the precipitation existing. In a second sampling method, thermal sample areas were selected based on the amalgamated center of initial convection formation areas and calculated on mean centers of initial reflectivity in 2 km radii buffer areas. The two sample methods were then individually tested against the mean temperature data from the 35 km study area buffer regions. Results were then reported as to significance of each event to each corresponding LANDSAT-5 imagery study area. The 2011 USGS National Land-Cover Dataset

(NLCD) was also used to examine possible connections to certain land-cover at the surface. The data set was downloaded from http://www.mrlc.gov/nlcd2011.php.

IV. RESULTS

This study examined the possible connection between the Indianapolis UHI effect and thunderstorms between the summer months of May to September for a ten year period (2002-2011 or 1,530 study days). Two forms of remote sensing data were used in order to determine that relationship. Statistical methods were used to determine if specific areas of thunderstorm formation were connected to warmer urban areas than cooler urban areas within Indianapolis. Results showed twenty-one events over eighteen study days of possible UHI thunderstorm initiation by the UHI (Table 4.1).

Day	Month	Year	Approx. Time of Initiation (GMT)	Approx. Time of Dissipation (GMT)
20	July	2011	19:33:43	21:56:21
5	August	2011	20:22:44	21:52:58
5	August	2011	21:11:28	21:52:58
19	August	2011	23:12:29	0:17:24
10	July	2010	11:12:37	12:49:47
10	July	2010	17:57:50	18:46:23
13	August	2010	22:15:41	0:57:29
2	September	2008	21:13:26	0:48:15
20	September	2008	20:17:12	21:42:45
20	September	2008	19:29:49	21:51:10
30	May	2006	16:24:38	17:38:15
29	July	2006	6:41:56	7:59:33
8	September	2006	18:36:36	20:20:38
24	June	2005	23:09:10	0:02:36
7	July	2005	0:24:36	1:53:25
9	August	2005	21:02:17	22:43:02
11	August	2005	3:03:08	4:14:51
2	July	2003	20:12:32	21:22:32
10	August	2003	15:49:02	16:58:32
14	August	2003	23:46:46	0:46:08
21	July	2002	21:25:06	22:59:19

Table 4.1: Temporal findings of possible urban induced thunderstorms from 2002-2011.

Temporal findings (Figure 4.1-4.3) show the years 2005 and 2011 having the most event days, with 2004, 2007 and 2009 having no event days. Monthly findings show August had the

most event days with seven, July second with six, September with three event days and the months of May/June with only one event per month. These monthly findings would make sense as the Indianapolis UHI would be more intense in the later summer months (JAS) rather than the early summer months of May and June. Hourly findings show 20Z (GMT) or 5PM EDT shows the highest frequency of initiation with only four events taking place over the nocturnal hours (Figure 4.1). Again this finding would make sense, as at 5PM the maximum temperature is reached and the amount of solar radiation the heat island is absorbing is at the highest.

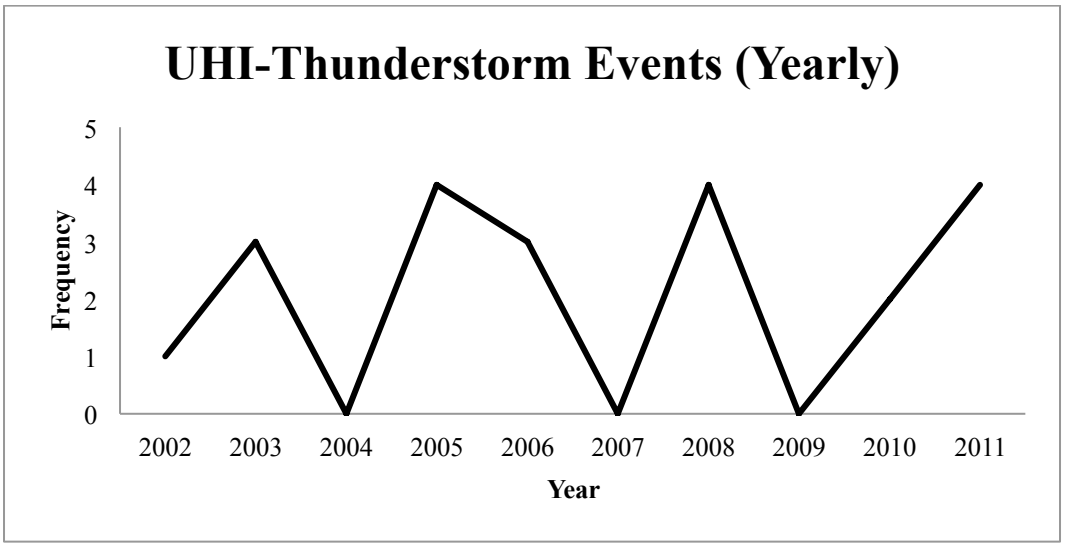

Figure 4.1: Yearly frequency of UHI-thunderstorm events in Indianapolis from 2002-2011

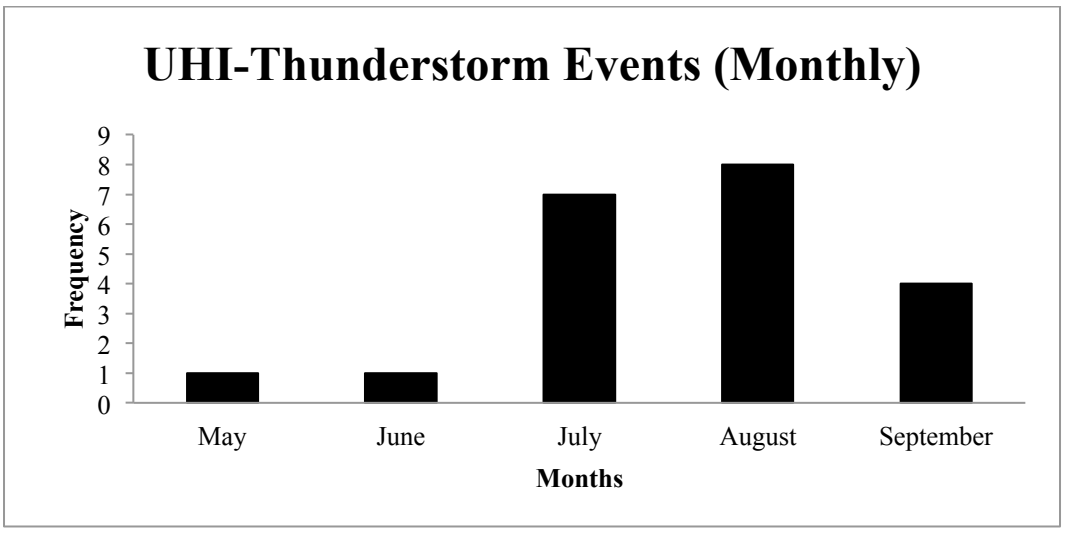

Figure 4.2: Monthly frequency of UHI- thunderstorm events in Indianapolis (2002-2011)

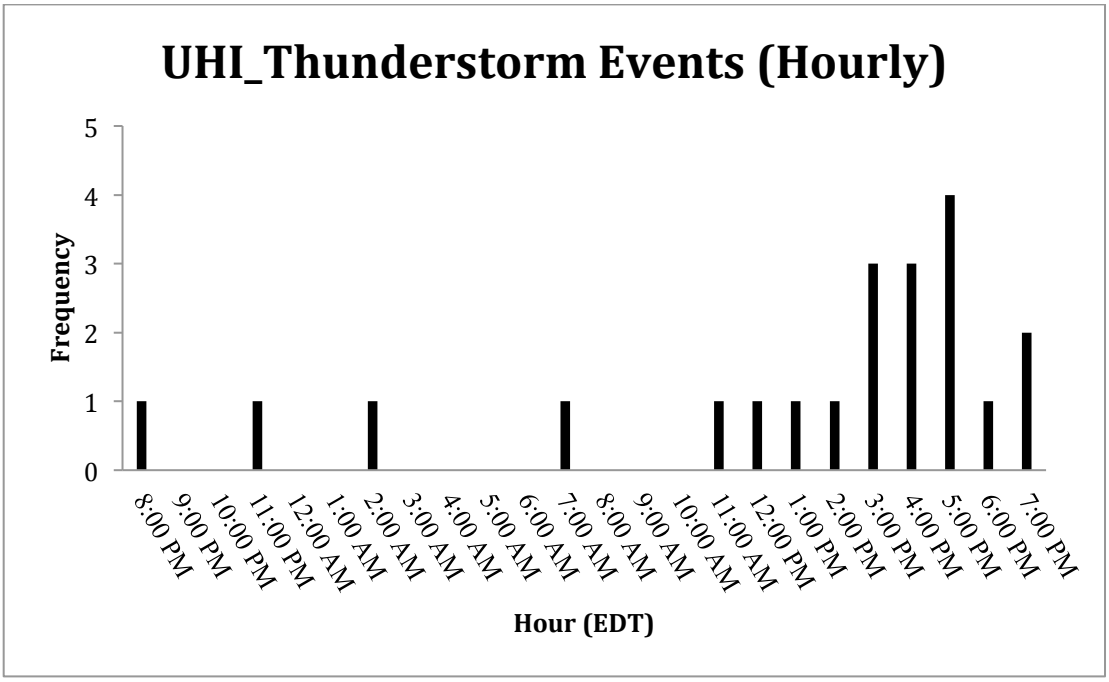

Figure 4.3: Hourly frequency of UHI induced thunderstorms for Indianapolis from 2002-2011

Initial scans were defined as the first 40dBZ signature on radar and the last 40dBZ scan was considered the dissipating scan or the last scan of the thunderstorm. All scans in between the initiation and dissipation stages were inputted into the WCT, filtered for reflectivity of 40dBZ or higher and converted into shapfiles for all 20 events. After all scans were converted to shapefiles, all reflectivity was combined into one shapefile using the merge function in ArcGIS 10. In addition to combining all reflectivity into one file, initial radar reflectivity polygon areas were processed to find the mean centers of that first reflectivity scan. The mean center is defined as the source of initial air parcel lift and therefore considered the source of convection. A 2 km buffer was drawn around this mean center point to sample. The reasoning behind this decision was to account for various sizes of air parcels at the surface. These "sample circles" were later used to clip the temperature raster layer from the LANDSAT-5 imagery.

Several LANDSAT-5 images were studied during the summer months (MJJAS) from May 2002 until September 2011. The average 16-day temporal passage of LANDSAT-5 allowed Indianapolis to be sampled on a regular basis throughout the summer study periods. In all, only

eleven satellite passes were cloud free and were viable for the analysis. Table 4.2 shows the assigned UHI-thunderstorm events to the corresponding satellite passage.

Storm Day	Assigned Image	LANDSAT Time (GMT)	Local Time (EDT)	Amount of Time Elapsed
7/20/2011	7/15/2011	16:12Z	12:12PM	5 Days
8/5/2011	7/15/2011	16:12Z	12:12PM	20 Days
8/5/2011	7/15/2011	16:12Z	12:12PM	20 Days
8/19/2011	9/1/2011	16:11Z	12:11PM	12 Days
7/10/2010	8/29/2010	16:13Z	12:13PM	49 Days
7/10/2010	8/29/2010	16:13Z	12:13PM	49 Days
8/13/2010	8/29/2010	16:13Z	12:13PM	16 Days
9/2/2008	9/24/2008	16:07Z	12:07PM	22 Days
9/20/2008	9/24/2008	16:07Z	12:07PM	4 Days
5/30/2006	4/28/2006	15:58Z	11:58AM	32 Days
7/29/2006	8/2/2006	16:16Z	12:16PM	4 Days
9/8/2006	8/2/2006	16:16Z	12:16PM	36 Days
9/8/2006	8/2/2006	16:16Z	12:16PM	36 Days
6/24/2005	4/25/2005	16:15Z	12:15PM	29 Days
7/7/2005	8/2/2005	16:15Z	12:15PM	26 Days
8/9/2005	8/2/2005	16:16Z	12:16PM	7 Days
8/11/2005	8/2/2005	16:16Z	12:16PM	9 Days
7/2/2003	7/25/2003	15:59Z	11:59AM	23 Days
8/10/2003	8/26/2003	16:00Z	12:00PM	16 Days
8/14/2003	8/26/2003	16:00Z	12:00PM	12 Days
7/21/2002	7/6/2002	15:58Z	11:58AM	15 Days

Table 4.2: Assigned LANDSAT-5 dates to corresponding UHI-thunderstorm events

On average, twenty days elapsed from the time before or after the UHI thunderstorm event and the satellite passage to record the UHI. The longest amount of days to elapse were forty-nine days (7 weeks) and the shortest temporal difference was four days. The images taken in between July and August 2010 were delayed longer due to extreme cloudiness on days when the LANDSAT-5 satellite passed over Indianapolis. The satellite also passed relatively on the same hour (12 PM EDT) for each day to reduce the effect of shadows biasing the temperature profile of the UHI.

After all satellite imagery was obtained and processed, the spatial analysis could finally begin on the data of both files types (UHI raster data and radar shapefiles). The analysis used a Geographic Coordinate System World Geodetic System 1984 (GCS WGS 1984) projection for data interpretation. This projection was used to account for the curvature of the earth and to account how NEXRAD radar scans the atmosphere on a spherical earth. The initial step to GIS interpretation was to clip the storm(s) of interest from the 40 dBZ filtered radar data. In some cases, ground clutter and thunderstorms outside the study area need to be eliminated via the spatial clip functions within ArcGIS. Figure 4.4 shows an example from a scenario on August 9th 2005 where ground clutter and extraneous radar reflectivity was eliminated.

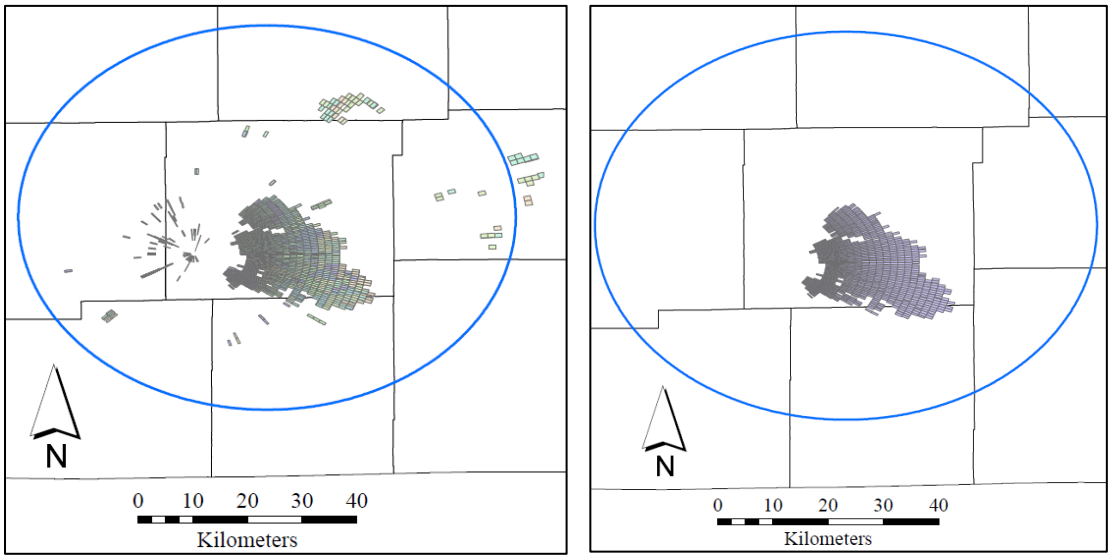

Figure 4.4: (Left) shows all imported radar reflectivity on August 9th 2005; (Right) shows the filtered 40 dBZ thunderstorm of interest for the August 9th 2005. The blue circle represents the study area of interest.

Once the storm or storms of interest were clipped the initial scan (the first instance where a 40 dBZ return was observed), the mean centers of the area of reflectivity was calculated using the mean center function within the spatial statistics tool pack within ArcGIS. An example of a mean center calculation is shown in figure 4.5 of the thunderstorm on August 9th 2005 (left). After the mean center was calculated a 2 km buffer was placed around this initial reflectivity study area to sample UHI areas around these initial radar returns also shown in figure 4.5 (right)

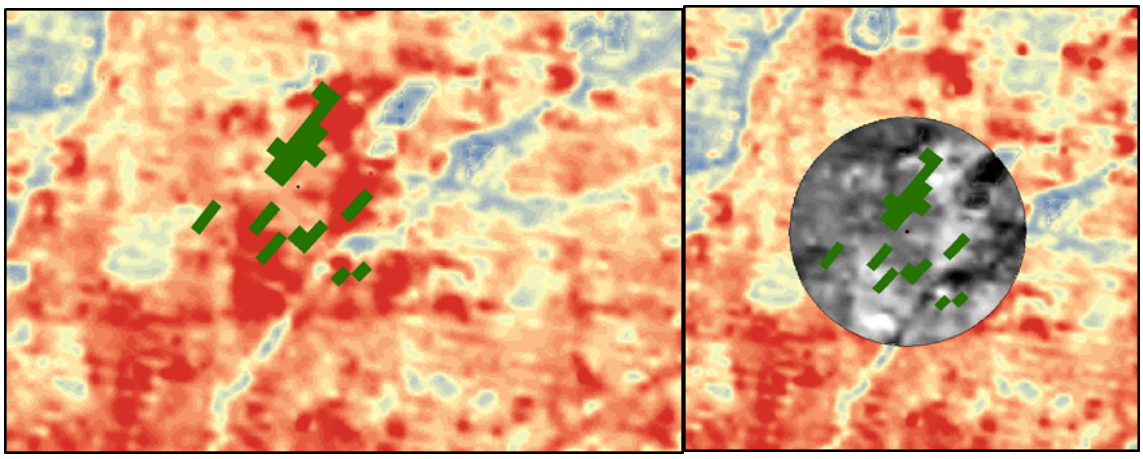

Figure 4.5: Thermal clip of thunderstorm reflectivity using the 2km buffer sample selection.

After initial areas were clipped and buffers were created for each of the eighteen thunderstorm days (20 events in total), samples could then be drawn from the UHI raster datasets. The LANDSAT-5 UHI imagery was cut to the 35 km research area where storm path and 2 km buffer areas could be sampled. These samples were then compared to the remaining UHI dataset. A difference of means test was used to determine statistically significant surface temperature differences between the two-samples (thunderstorm UHI areas and UHI study area) for both sample types (storm path and 2 km initiation areas). Once clipped, raster data for the UHI study areas and the samples were converted into numerical datasets to be used within a statistical package (SPSS) for analysis.

Results from the eleven UHI study areas are in table 4.3. The data shows confirmation there is variability in the Indianapolis UHI from April until September. On average the July UHI was the largest in range and in magnitude, while April and September showed in lowest range and minimum average temperatures. In addition to successfully identifying the magnitude of the heat island, visual confirmation using a fixed scale showed variation in space of the UHI. Figure 4.6 exhibits this change from April 2006, August 2005 and September 2008. The mean temperature values of the 35 km study area were used to test whether storm path and initiation samples drawn from these areas were significant.

35 km UHI Areas	Max (°C)	Min (°C)	Range (°C)	Mean (°C)	S.D. (°C)
April 28 2006	33.33	17.65	15.68	23.68	2.9
Aug 2 2006	36.95	16.2	20.75	23.17	2.3
Sept 24 2008	40.07	10.61	29.46	19.61	2.2
Sept 1 2011	35.26	9.64	25.62	21.56	2.2
July 6 2002	42.75	9.08	33.67	23.05	3.2
July 25 2003	44.26	13.89	30.37	20.84	3.2
July 15 2011	43.95	13.45	30.5	21.62	3.2
Aug 29 2010	36.88	14.62	22.26	21.93	2.1
Aug 26 2003	37.36	13.63	23.73	21.36	2.2
April 25 2005	36.39	16.64	19.75	22.43	2.5
Aug 2 2005	36.7	14.54	22.16	21.63	2.6
Total	38.5	13.6	24.9	21.9	2.6

Table 4.3: Descriptive statistics of the 35 km study areas from 2002 to 2011.

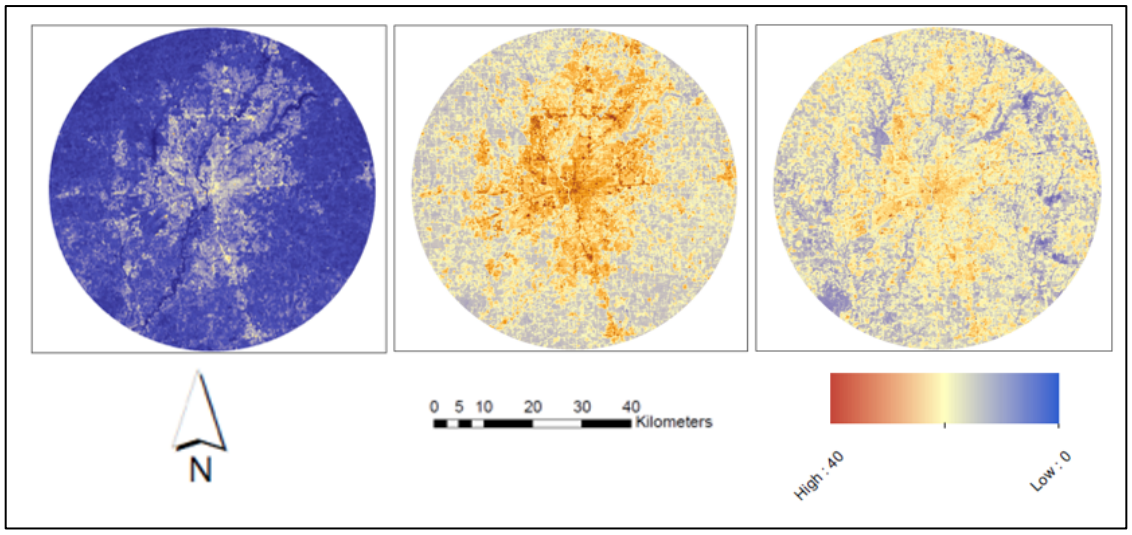

Figure 4.6: Visual variations in the Indianapolis UHI from April (L), Aug (C), and Sept (R).

UHI sampling results showed promising for both storm path and initiation methods. The majority of the thunderstorms researched in this analysis passed over the warmest sections of Central Indianapolis but did not initiate over the hottest portion of the city. Therefore, some bias may be in the results with the storm path method. The 2 km buffer sampling method showed less promising results as 43% of thunderstorms initiated in areas without significant warming. Only four thunderstorms initiated in the warmest section of the city, the rest formed on the periphery

and borders along the cities. Similar results were seen in Atlanta with the 1996 Olympic case studies where storms developed on the Eastern (downwind) side of Atlanta (Bornstein and Lin 2000). Tables 4.4 and 4.5 display the results from both sampling methods for all 21 events from 2002 until 2011.

Storm Date	Storm Path Max Temp	Storm Path Mean Temp	Study Area Mean Temp	Difference Mean Temp	Storm Path z-scores	Storm Path p-value
7/20/2011	31.7	26.2	21.6	4.6	1.43	0.076
8/5/2011	39.7	28.1	21.6	6.5	1.59	0.056
*8/5/2011	37.4	28.6	21.6	7.0	2.18	0.015
*8/19/2011	29.7	27.3	21.6	5.7	2.63	0.004
*7/10/2010	34.2	27.8	21.9	5.9	2.78	0.003
*7/10/2010	33.2	26.8	21.9	4.9	2.33	0.010
*8/13/2010	35.4	26.7	21.9	4.8	2.28	0.011
*9/2/2008	38.1	25.0	19.6	5.4	2.47	0.007
*9/20/2008	32.0	26.3	19.6	6.7	3.05	0.001
9/20/2008	33.2	25.5	19.6	5.9	2.72	0.003
5/30/2006	39.8	25.0	23.7	1.3	0.46	0.323
*7/29/2006	32.1	29.1	23.2	5.9	2.90	0.002
*9/8/2006	36.0	30.3	23.2	7.1	3.04	0.001
*6/24/2005	36.7	30.4	22.4	8.0	3.22	0.001
*7/7/2005	32.8	29.0	21.6	7.4	2.85	0.002
*8/9/2005	36.5	29.9	21.6	8.3	3.19	0.001
*8/11/2005	36.0	28.3	21.6	6.7	2.58	0.005
*7/2/2003	44.3	29.7	20.8	8.9	3.87	0.000
*8/10/2003	31.3	27.7	21.4	6.3	2.91	0.002
*8/14/2003	36.5	31.2	21.4	9.8	4.57	0.000
*7/21/2002	40.9	30.7	23.1	7.6	2.40	0.008

Table 4.4: Results of a one-sample/one-tailed t-test. Statistically significant results have an asterisk denoted by the storm date. All temperatures are reported in degrees Celsius.

August 14, 2003 had the largest temperature difference with a 9.8° C difference between the storm path and the remaining 35 km radius study area. The August 2003 is interesting since the storm initiated from the city center of Indianapolis. In addition to having such a large temperature gradient between these areas, the results also show a non-existent gradient with some

of the event storm paths. For instance the May 2006 storm only had a 1.3° C difference between the storm path and remaining sample. This thunderstorm also developed upwind of Indianapolis over the Speedway, Indiana area and the Indianapolis Motor Speedway. Therefore something other or in addition to thermal gradients may be causing initiation (i.e. surface roughness or GCCN) for some of these cases. Figure 4.7 shows all radar reflectivity used in storm path selection. Note: prior to 2008 the radar sampled the atmosphere at 1 km resolution. After 2008, super resolution radar sampling at 250 meters began. In any case, this did not impact sampling of the UHI for statistical analysis.

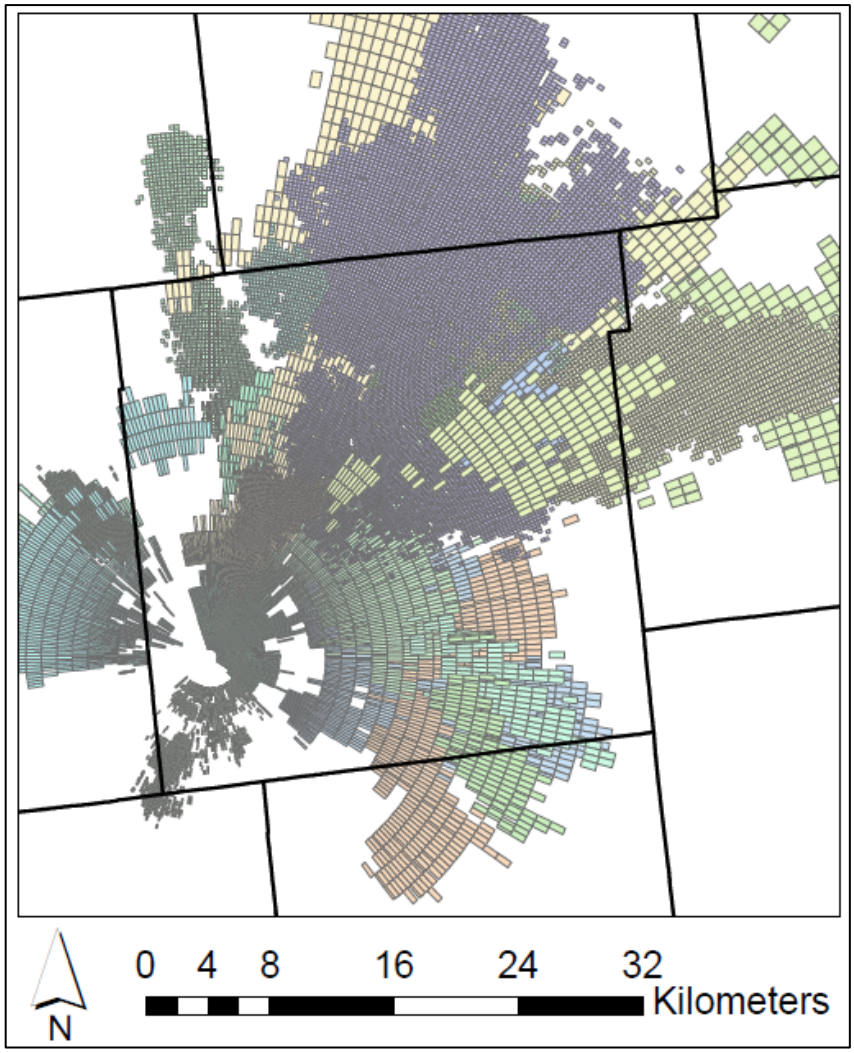

Figure 4.7: All 21 storm paths overlaid by an Indiana county shapefile for reference

Storm Day	I.P. Max (°C)	I.P. Mean Temp	Study Area Mean Temp	Difference Mean Temp	I.P. z-score	I.P. p-value
*7/20/2011	23.8	26.1	21.6	4.5	2.09	0.018
*8/5/2011	33.5	26.5	21.6	4.9	1.80	0.036
*8/5/2011	29.1	27.2	21.6	5.6	2.71	0.003
*8/19/2011	29.6	24.5	21.6	2.9	1.99	0.023
7/10/2010	29.2	24.9	21.9	3.0	1.40	0.081
7/10/2010	33.0	24.4	21.9	2.5	1.23	0.110
*8/13/2010	29.1	25.6	21.9	3.7	1.88	0.030
*9/2/2008	31.5	24.2	19.6	4.6	2.13	0.016
*9/20/2008	33.0	23.5	19.6	3.9	2.03	0.021
9/20/2008	35.5	22.2	19.6	2.6	1.40	0.080
5/30/2006	23.1	27.6	23.7	3.9	0.04	0.518
*7/29/2006	33.1	25.9	23.2	2.7	2.11	0.017
9/8/2006	32.3	25.2	23.2	2.0	1.11	0.133
6/24/2005	35.4	25.7	22.4	3.3	1.49	0.068
*7/7/2005	34.1	25.9	21.6	4.3	2.72	0.003
*8/9/2005	32.5	28.3	21.6	6.7	3.23	0.001
*8/11/2005	32.1	26.6	21.6	5.0	2.48	0.007
7/2/2003	32.0	25.4	20.8	4.6	1.61	0.054
8/10/2003	35.3	24.1	21.4	2.7	1.63	0.052
*8/14/2003	32.5	25.2	21.4	3.8	2.88	0.002
7/21/2002	35.5	27.7	23.1	4.6	1.62	0.053

Table 4.5: 2 km initiation buffer sample areas in degrees Celsius. Dates with asterisks denote statistically significant differences in mean temperature areas to reaming study areas.

Only 57% of thunderstorm initiation locations were statistically different in surface temperatures. August 9, 2005 had the largest 2 km buffer temperature difference while September 8, 2006 had the lowest temperature average between the sample area and the study area. In total the average mean temperature difference was 3.6°C from all initiation areas and study areas. The August event formed directly over the city center of Indianapolis, allowing the sample to include all warm areas of the city of Indianapolis. The September event formed over the NE portion of Marion County near the Geist reservoir. Once again, the evidence shows other forcing may be at play with these initiation areas. Therefore land-cover types were examined to see if further

patterns or land-cover type may be at play. Figure 4.8 displays all 2 km buffer sample areas with respect to Indianapolis.

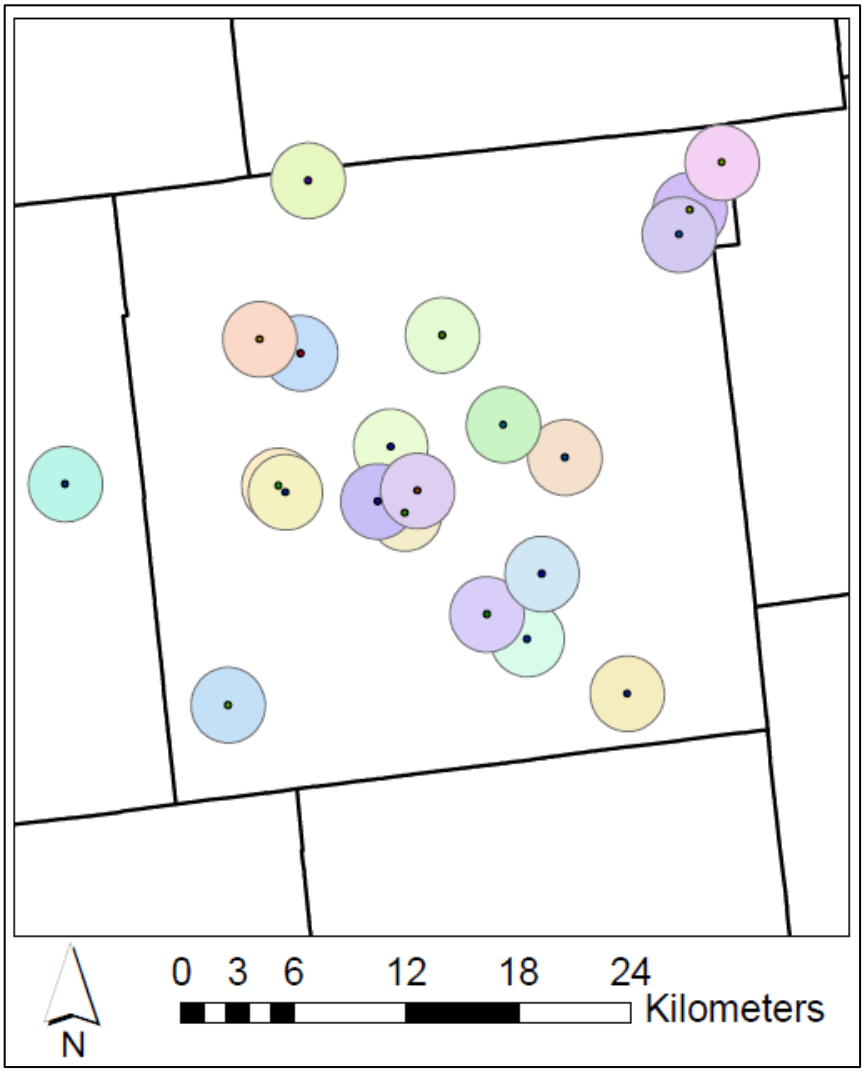

Figure 4.8: 2 km initiation sample areas around Indianapolis. Mean centers are the point within the circular buffers depicting the center of initial reflectivity.

Initiation patterns tend to show heavier concentrations of initiation to the south and east of the downtown Indianapolis area. Several initiation areas overlapped, especially around the city center, Speedway and Beach Grove locations in Marion County. A further analysis was conducted to determine patterns with land-cover type using the 2011 US National Land-Cover Dataset (NLCD) of the Indianapolis area. Unlike thermal remote sensing imagery, only one land-cover dataset was used to compare land-cover type in a constant study area image.

The 2011 NLCD file was clipped to the 35 km study and initial analysis of study area land-cover type was calculated by counting the number of pixels for each sixteen-class land-cover type. Percentages were then calculated for the study area and then compared to clipped 2 km initiation areas. Fifteen of the twenty land cover type classes were present in the 35 km study area, with developed open space (light pink) being the most predominate land-cover type by area.

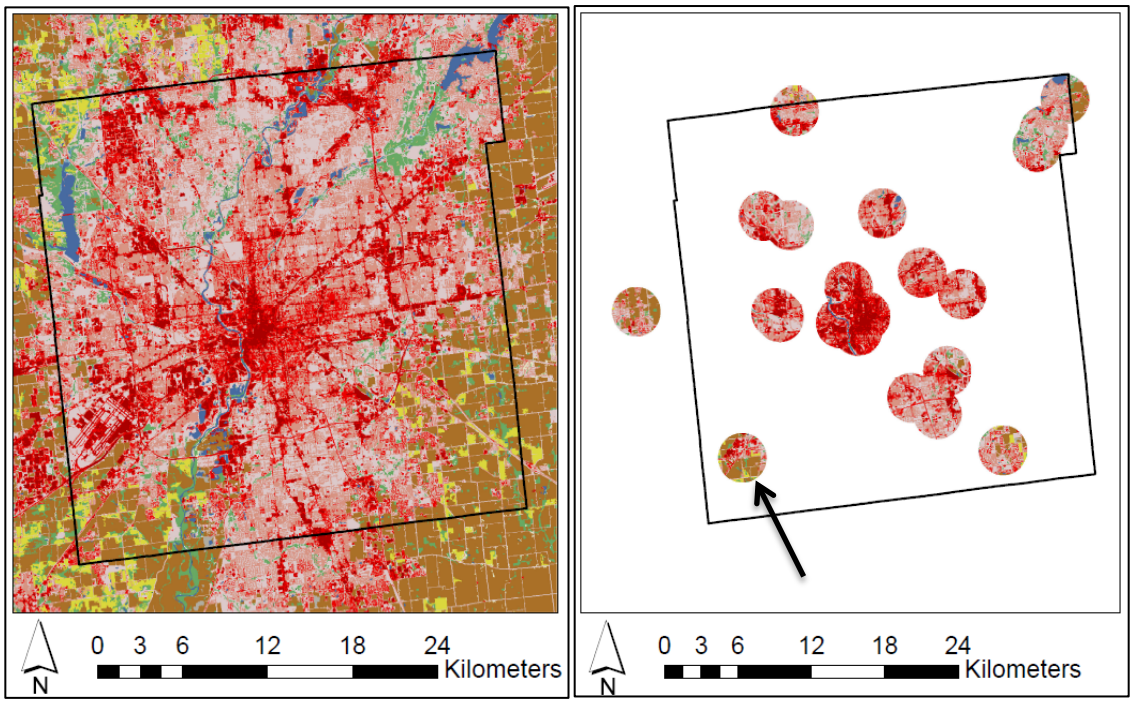

Figure 4.9: An image displaying the 2011 NLCD land-cover type for Indianapolis and the clipped study regions sampled from the 2 km buffer areas.

Sampled regions showed patterns of discreet boundaries between land-cover types in all sample regions. An example of this land-cover change is shown above in the lower left corner of Marion County (black arrow). A drastic change from crops and pasture land to low intensity development is apparent in this area. In other examples, mostly in central Marion County, the land-cover type changes from low/middle development to high level development depicted by the change from light pink to dark red in the right-hand map above. Examining the land-cover type further, found that low intensity development was the predominate land-cover type (33% by area) in the twenty-one 2 km buffer regions. Followed by open space (24%), medium intensity

development (21%). These findings build upon previous studies (Niyogi et al. 2011) supporting land-surface heterogeneity and land-surface boundaries may play an important role in initiating thunderstorms in urban environments such as Indianapolis.

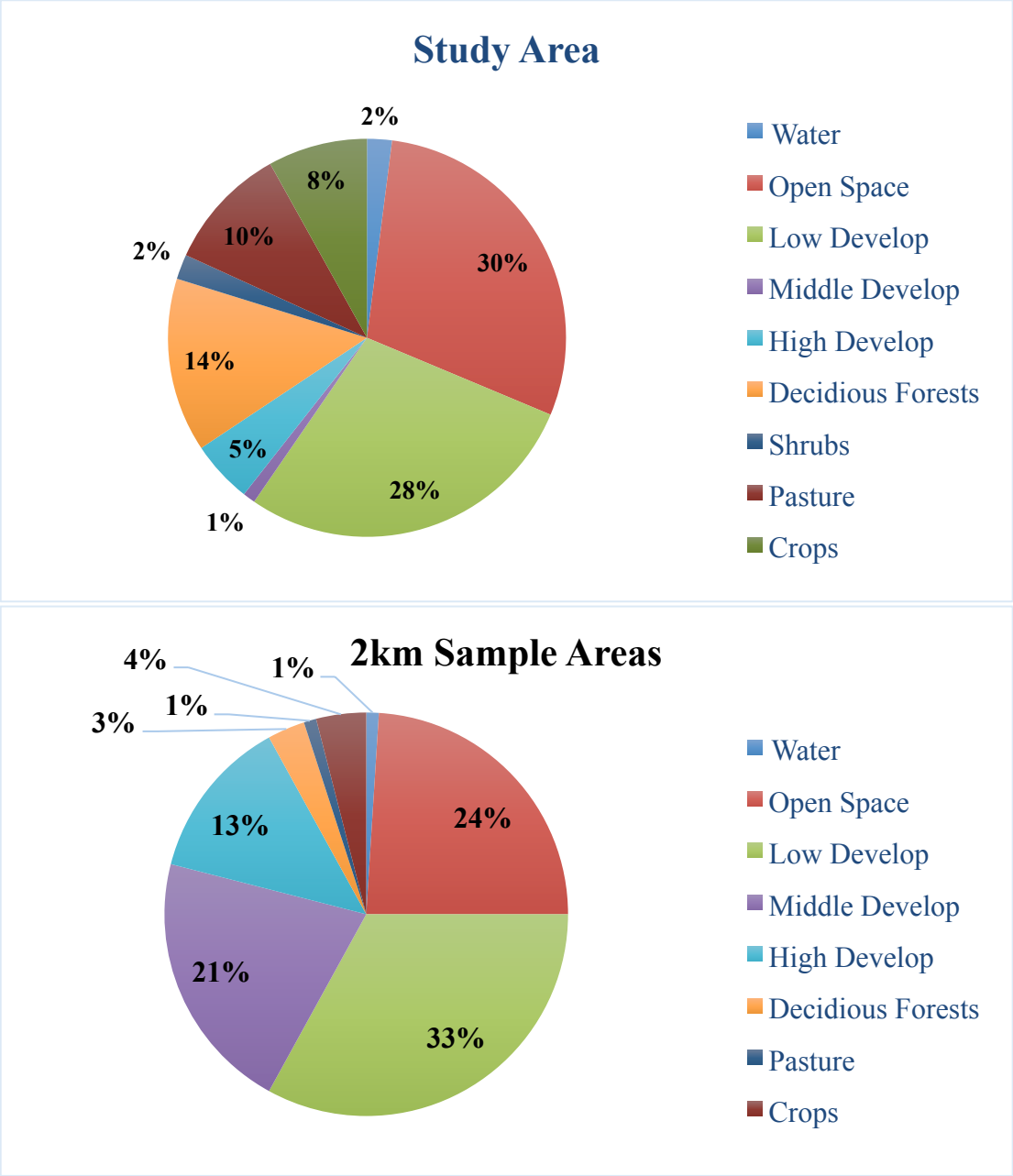

Figure 4.10: Charts depicting land-cover type by class in the entire study area (top); and the 21-2km sample areas (below).

V. CONCLUSION

This analysis studied the relationship of thunderstorms with the Indianapolis UHI. An additional analysis was conducted to see if distinct patterns of convection followed or initiated over certain land-cover types. The study attempted to track the spatial and temporal variation of the Indianapolis UHI and the pattern of thunderstorms over a ten-year period from May 2002 until September 2011. The consequences of this analysis showed the heat island did morph and intensify throughout the warm season months in Indianapolis. In addition, the study found twenty-one events happened over a ten-year period, with August exhibiting the most events in a periodic pattern during this time series. These rare events take place mostly in the late afternoon hours when daytime heating is the warmest and the UHI magnitude begins to release excess heat into the atmosphere. Results also showed there is a marked difference (90% of the time) in areas where thunderstorms track as temperatures below thunderstorm paths are higher than surround study areas. Moreover, results from initiation locations in 2 km initiation areas showed a 57% occurrence of a warmer surface being directly below the thunderstorm initiation area. These two drastic outcomes showed mixed results but, the results were helpful at gaining further evidence that the UHI and thunderstorm relationship is complicated, yet tied with various parameters (i.e. roughness length, topography, pollution, GCCN) not solely tied to forcing from the UHI. Factors such as surface roughness and variations in fluxes due to land-surface type may allow additional lift to the urban environment needed for thunderstorm formation. For this reason land-cover was also examined to determine if possible land-cover types could effect thunderstorm formation.

The land-cover type analysis with thunderstorms initiation areas showed, low intensity development is important. Low-intensity land-cover such as single-family housing is predominate in the land-cover types along with open space and medium intensity land-cover with 50-79% impervious surfaces. These two land-cover types encompass 54% of the land-cover in each 2 km buffer areas. Still there needs to be improvement on understanding the micro-scale processes (small than 2 km) in these environments.

Finally, there are many opportunities at furthering this proceeding research area and topic. First, various radius study areas larger and smaller are need to be tested and compared to the 2 km study analysis. Spatial clustering and kernel density analysis would help in these endeavors. A second improvement and research opportunity include utilizing higher spatial and temporal resolution platforms and equipment to understand the complex heterogeneity of the urban surface. Newer platforms including LANDSAT-8, AVHRR, IKONOS and drone technology would allow for better data collection in spatial (less than 30m) and temporal (less than 16 day, 20 day for this analysis) scales. Third, other cities other than Indianapolis need to confirm the same results found in this analysis. Cities predominately in low-intensity land-cover types such as Minneapolis, Kansas City, Omaha and St Louis would be good candidates.

Works Cited

Adegoke, J. O., and K. P. Gallo, 2004: On the relation between surface spatial heterogeneity and climate prediction: Insights from the integration of fine resolution satellite land information into mesoscale climate models. Preprints, Eighth symp. on integrated observing and assimilation systems for atmosphere, oceans, and land surface, Seattle, WA, Amer. Meteor. Soc.

Andreae, M. O., D. Rosenfeld, P. Artaxo, A. A. Costa, G. P. Frank, K. M. Longo, and M. A. F. Silva-Dias, 2004: Smoking rain clouds over the Amazon. *Sci*ence, **303**, 1337-1342.

Ashley, W. S., M. L. Bentley, and J. A. Stallins, 2012: Urban-induced thunderstorm modification in the Southeast United States. *Climatic Change,* **113**, 481-498.

Bentley, M. L., Ashley, W.S. and J. A. Stallins, 2010: Climatological radar delineation of urban convection for Atlanta, Georgia. *Int. J. Climatol*., **30**, 1589–1594.

Bornstein, R., and Q. Lin, 2000: Urban heat islands and summertime convective thunderstorms in Atlanta: Three case studies. *Atmos. Environ*., **34**, 507–516.

Bornstein, R. D., and M. LeRoy, 1990: Urban barrier effects on convective and frontal thunderstorms. Extended Abstracts, *Fourth conf. on mesoscale processes*, *Amer. Meteor. Soc.,* 120–121.

Bornstein, R. D., 1968: Observations of the Urban Heat Island Effect in New York City. *J. Appl. Meteor.*, **7**, 575–582.

Brown, M. E., and D. L. Arnold, 1998: Land–surface–atmosphere interactions associated with deep convection in Illinois. Int. J. Climatol., 18, 1637–1653.

Carlson T N, Augustine J A, Boland F E, 1977: Potential application of satellite temperature measurements in the analysis of land use over urban areas. *Bull. Amer. Meteor. Soc*., **58** 1301–1303.
Changnon, S. A., 1981: METROMEX: *A Review and Summary. Meteor. Monogr*., No 40, Amer. Meteor.Soc.

Cotton, W.R., and R. A. Pielke, 2007: Inadvertent human impacts on regional weather and climate. *Human Impacts on Weather and Climate*, 2nd ed., Cambridge University Press, 73-148.

Diem, J. E., and D. P. Brown, 2003: Anthropogenic impacts on summer precipitation in central Arizona, U.S.A. *Prof. Geogr.,* **55** (3), 343–355.

Dixon, P.G., and T. L. Mote, 2003: Patterns and causes of Atlanta's urban heat island-initiated precipitation. *J. Appl. Meteor.*, **42**, 1273-1284.

Gunn, Ross, B. B. Phillips, 1957: An experimental investigation of the effect of air pollution on the initiation of rain. *J. Meteor.,* **14**, 272–280.

Kalkstein, L.S., C.D. Barthel, J.S. Greene and M.C. Nichols, 1996: A new spatial synoptic classification: application to air mass analysis., *Int. J. Climatol*., **16**, 983-1004

Lacke M.C., T.L. Mote, J.M. Shepherd, 2009: Aerosols and associated precipitation patterns in Atlanta. *Atmos. Environ*., **43**, 4359-4373.

Loose, T., and R. Bornstein, 1977: Observations of mesoscale effects on frontal movement through an urban area. *Mon. Wea. Rev*., **105,** 563–571.

Miao, Shiguang, Fei Chen, Margaret A. LeMone, Mukul Tewari, Qingchun Li, Yingchun Wang, 2009: An observational and modeling study of characteristics of urban heat island and boundary layer structures in Beijing. J. Appl. Meteor. Climatol., 48, 484–501.

Mills, G 2008: Luke Howard and The Climate of London. *Weather,* **63,** 153-157.

Multi-Resolution Land Characteristics Consortium (MRLC), cited 2014: Multi-Resolution Land Characteristics Consortium [Available online at http://www.mrlc.gov/nlcd06_data.php]

Myrup, L. O., 1969: A Numerical Model of the Urban Heat Island. *J. Appl. Meteor*., **8**, 908–918

National Aeronautic and Space Administration (NASA), 2009: Landsat 7 Science Data Users Handbook, Chapter 11, 117-120

National Climatic Data Center (NCDC), cited 2014: NCDC NEXRAD Data Inventory Search. [Available online at http://www.ncdc.noaa.gov/nexradinv/covmaps.jsp?id=KIND]

Niyogi, D., P. Pyle, M. Lei, S. P. Arya, C. M. Kishtawal, M. Shepherd, F. Chen, B. Wolfe, 2011: Urban Modification of Thunderstorms: An observational storm climatology and model case study for the Indianapolis urban region. *J. Appl. Meteor. Climatol.*, **50**, 1129–1144.

Niyogi D., Pielke R.A., Adegoke J., Chang HI., Chase T., Douglas E., Gupte. M, Marshall C, Matsui T, Pyle P, Shepherd M. 2006: Considering the role of aerosols and land-atmosphere interactions. Related to agriculture and urbanization in climate studies. Amer. Assoc. Geogr. Annual Meeting, Chicago, March 2006.

Oke, T. R., 1997: Urban climates and global environmental change. Applied Climatology R.D. Thompson and A. Perry, Eds., Routledge, 273-287.
Oke, T. R., 1987: Boundary Layer Climates. 2nd Ed. London: Methuen.

Oke, T.R., 1981: Canyon geometry and the nocturnal urban heat island: comparison of scale model and field observations, *J. Climat*., **1**, 237-254.

Oke, T.R. 1973: City size and the urban heat island. *Atmo Environ*. **7**: 769-779.

Orklanski, I., 1975: A rational subdivision of scales for atmospheric processes. *Bull. Amer. Meteor. Soc.,,* **56**, 527-530.

Price, J. C., 1979. Assessment of the Urban Heat Island Effect through the Use of Satellite Data. *Mon. Wea. Rev*., **107**, 1554-1557.

Ramanathan, V., P. J. Crutzen, J. T. Kiehl, and D. Rosenfeld, 2001: Aerosols, climate, and the hydrological cycle. *Science*, **294**, 2119–2124.

Rao, P. K., 1972: Remote sensing of urban heat islands from an environmental satellite, *Bull. Amer. Meteor. Soc.,* **53**, 647−648.

Rose, L. S., J. A. Stallins, M. L. Bentley, 2008: Concurrent cloud-to-ground lightning and precipitation enhancement in the Atlanta, Georgia (United States), Urban Region. *Earth Interact.,* **12,** 1–30.

Rosenfeld D., U. Lohmann, G.B. Raga, C.D. O'Dowd, M. Kulmala, S. Fuzzi, A. Reissell, M.O. Andreae, 2008: Flood or drought: How do aerosols affect precipitation? *Science*, **321**, 1309-1313

Rosenfeld, D., 2007: New insights to cloud seeding for enhancing precipitation and for hail suppression. *J. Wea. Mod*., **39**, 61-69.

Rosenfeld D. and C. W. Ulbrich, 2003: Cloud microphysical properties, processes, and rainfall estimation opportunities. *Radar and Atmospheric Science: A Collection of Essays in Honor of David Atlas*, *Meteor. Monogr.* **52**, 237-258.

Rosenfeld, D., 2000: Suppression of rain and snow by urban air pollution. *Science,* **287**, 1793–1796.

Rosenfeld, D., 1999: TRMM Observed first direct evidence of smoke from forest fires inhibiting rainfall. *Geophys. Res. Lett*. **26**, 3105-3108

Rozoff, C., W. R. Cotton, and J. O. Adegoke, 2003: Simulation of St. Louis, Missouri, land use impacts on thunderstorms. *J. Appl. Meteor*., **42**, 716–738.

Salamanca F., Martilli A., Tewari M., Chen F., 2011: A study of the urban boundary layer using different urban parameterizations and high-resolution urban canopy parameters with WRF. *J. Appl. Meteor. Climatol.,* **50,** 1107–1128.

Scheitlin, K.N. and P. G. Dixon. 2010: Diurnal temperature range variability due to land cover and airmass types in the Southeast. *J. Appl. Meteor*. **49**, 879-888

Shepherd, J. M., 2005: A review of current investigations of urban-induced rainfall and recommendations for the future. *Earth Interactions* **9**, 1–27.

Shepherd, J.M., H. Pierce, and A.J. Negri, 2002: Rainfall modification by major urban areas: Observations from spaceborne rain radar on the TRMM satellite*. J. Appl. Meteor.,* **41**, 689-701

Sheridan, S.C., 2002: The re-development of a weather type classification scheme for North America*, Int.J. Climatol*. **22**, 51-68

Sobrino, J.A., Jimenez-Munoz, J.C., & Paolini, L., 2004: Land surface temperature retrieval from LANDSAT TM 5. *Remote Sensing of Environment*, 434-440

Stallins JA, Bentley ML. 2006. Urban lightning climatology and GIS: an analytical framework from the case study of Atlanta, Georgia. *Appl. Geo.* **26**: 242–259

Thielen, J., W. Wobrock, A. Gadian, P. G. Mestayer, and J.-D. Creutin, 2000: The possible influence of urban surfaces on rainfall development: A sensitivity study in 2D in the mesogamma scale. *Atmos. Res*.,**54**, 15–39.

Tsonis, A. A., 2007: Atmospheric Thermodynamics. 2nd ed. Cambridge University Press. 55 pp
University Cooperative of Atmospheric Research (UCAR), cited 2014: Image Archive. [Available online at http://locust.mmm.ucar.edu/.]

United Nations (2007) Population prospects: The 2006 revisions and world urbanization prospects: The2007 revision. Population division of the Department of Economic and Social Affairs of the United Nations Secretariat.

Van den Heever, S.C., and W. R. Cotton, 2007: Urban Aerosol Impacts on Downwind Convective Storms. *J. Appl. Meteor. Climatol*., **46**, 828–850.

Weng, Q., Lu, D., Schubring, J., 2004: Estimation of land surface temperature–vegetation abundance relationship for urban heat island studies. Remote Sensing of Environment, 467-483

CURRICULUM VITAE

Kelly D. Boyd

PROFESSIONAL EXPERIENCE

2014-2013 **Instructor of Record (Graduate Teaching Assistant)**
Mississippi State University
GR 1123 World Geography (2 Sections; 200 students)
Starkville, MS

Summer 2014 **Graduate Research Assistant**
Mississippi State University
I worked on wind measurement assessment for the Mississippi Department of Transportation, specifically determining the measurement of prototype equipment for spray truck applications.
Starkville, MS

2013-2011 **Graduate Teaching Assistant**
Ball State University
GEO-101L Physical Geography Laboratory (3 Sections; 60 students)
Muncie, IN

Summer 2011 **Summer Graduate Internship (Volunteer)**
National Weather Service Forecast Office (KIND)
Indianapolis IN

EDUCATION

2015 **Department of Geography, Indiana University**
Master of Science, Geographic Information Systems

Thesis Topic: **Identifying Enhanced Urban Heat Island Convection Areas for Indianapolis, Indiana**
Advisor: Dan Johnson, Ph.D.

2013 **Department of Geography, Ball State University**
Master of Science, Geography w/concentration in Applied Atmospheric Science

Thesis Topic: **An Observational Climatology of Urban Initiated Thunderstorms across the Nashville Metropolitan Area**
Advisor: Jill Coleman, Ph.D.

2010 **School of Environmental & Public Affairs, Indiana University**
Bachelor of Science, Public Affairs Management

Capstone: **"Coworking as an Effective Solution for the Vacant Space at the Harrison Center for the Arts"**
Advisor: Jeffrey Paine, Ph. D.

CONFERENCES ATTENDANCE & PRESENTATIONS

2014	**International Conference in Biometeorology** Cleveland, Ohio
2014	**Association of American Geographers Annual Meeting** Tampa, Florida Identifying Enhanced Urban Heat Island Convection Areas for Indianapolis, Indiana using remote sensing methods
2014	**94th Annual American Meteorological Society** Atlanta, Georgia An Observational Climatology of Urban Initiated Thunderstorms across the Nashville Metropolitan Area
2014	**Southeast Severe Weather Symposium** Starkville, Mississippi
2012	**International Conference in Urban Climate** Dublin, Ireland
2012	**West Lake/East Lake Join Meeting for the AAG** DeKalb, Illinois
2008-2012	**Central Indiana Severe Weather Symposium** Greenwood, Indiana

PROFESSIONAL AFFILIATIONS

2013 – present	**International Society for Biometeorology**
2013 – present	**Association of American Geographers**
2008 – present	**American Meteorological Society**
2010 – present	**International Association for Urban Climate**

DATA ANALYSIS APPLICATIONS EXPERTISE

Geographic Information Systems and Remote Sensing Platforms: Maptitude, ArcGIS, QGIS, ERDAS

Weather/Climate programs and data types: NOAA Weather and Climate toolkit, BUFKIT, METAR, Gibson Ridge Software visualization packages, experience with Level I and II radar software data types as well as NCDC raw climate data sets (.DAT, CLASS, MADIS)

Mathematics: MATLAB & Mathematica

Statistical: R, SPSS & WinBugs